October 2018

Surface Functionalization of Fabrics and Threads for Smart Textiles

Morgan Baima

Recommended Citation

Surface Functionalization of Fabrics and Threads for Smart Textiles

A Dissertation Presented

by

MORGAN L. BAIMA

Submitted to the Graduate School of the University of Massachusetts Amherst in partial
fulfillment of the requirements for the degree of

DOCTOR OF PHILOSOPHY

CHEMISTRY

September 2018

Surface Functionalization of Fabrics and Threads for Smart Textiles

A Dissertation Presented

by

MORGAN L. BAIMA

Approved as to style and content by:

_____

Trisha Andrew, Chair

_____

Dhandapani Venkataraman, Member

_____

S. Thai Thayumanavan, Member

_____

Anthony D. Dinsmore, Member

_____

Ryan Hayward, Member

_____

Richard Vachet, Department Head
Chemistry Department

DEDICATION

To my loving [and crazy] husband, who followed me across the country twice and put his own education on hold so that I could achieve my academic goals.

ACKNOWLEDGEMENTS

ABSTRACT

SURFACE FUNCTIONALIZATION OF FABRICS AND THREADS FOR SMART
TEXTILES

SEPTEMBER 2018

MORGAN L. BAIMA, B.A., ST. EDWARD'S UNIVERSITY

M.A., UNIVERSITY OF WISCONSIN MADISON

Ph.D., UNIVERSITY OF MASSACHUSETTS AMHERST

Directed by: Professor Trisha L. Andrew

The future of electronics is moving toward wearable devices and therefore requires a shift away from hard, inflexible materials towards fibers, threads, and fabrics that conform to the shape of the body. Therefore new methods for incorporating textiles as electronic components are needed to replace conventional processing techniques used with smooth, flat substrates like glass, silicon, and many polymers. Toward this end, this work investigates different methods that can be used to tune textile surfaces for electronic functionality, including weaving, solution grafting, and initiated chemical vapor deposition (iCVD). While all of these methods were used to make triboelectrically-active textiles, iCVD combined with simple solution chemistry was also used to synthesize ionically conductive thin films on textiles for solid-state electrolytes. In general these methods elucidate facile pathways towards smart clothing fabrication.

TABLE OF CONTENTS

LIST OF TABLES

LIST OF FIGURES

CHAPTER 1

INTRODUCTION

1.1 Introduction to Electronic Textiles

Electronic textiles (E-textiles) or smart textiles generally refer to textiles that have an electronic component, wherein they conduct electricity or serve as the platform for components with electronic functions. Applications of these materials include health and fitness sensing, [1–5] temperature control [6], electrical switches [7], energy harvesting and storage, [8] communication, [9–12] and illumination. [13–15] Whether their purpose is to improve diagnostics or simply act as a wearable flashlight, it is clear that wearable technologies are moving towards more comfortable, flexible platforms, the most comfortable and flexible being textiles.

From a materials perspective, incorporating electronics into textiles has proven a significant challenge. In particular, problems arise where the typical plastics and metals used for even the thinnest of electronic devices are bulky in comparison to fabrics, ultimately limiting placement on the garment and changing the way a garment feels and moves. Not only are these types of smart garments uncomfortable and often awkward, but they cannot be laundered because conventional dip-coating, dyeing, and metal plating methods result in poor adhesion to the textile. On the other hand, encapsulating small electronic components in soft silicones or other flexible polymers allows for laundering and exposure to humidity but not breathability. For these reasons, smart textiles have not been widely adopted for commercial use.

These issues make clear the fact that conventional methods for electronics fabrication are insufficient for the creation of the next generation of smart textiles. Instead, new methods must be explored in order to preserve the flexibility and feel of the textile but also enable electronic function. For example, rather than placing conventional electronics into clothing, a better solution would be to make conventional fabrics and threads themselves electronic. One plausible way to do so is to use the textile as the substrate and modify the

1

surface such that the clothing maintains its familiar look, feel, and flexibility but also serves a functional purpose. To this end, the goal of this thesis work is to investigate different ways of modifying textile surfaces towards electronically functional ("smart") fabrics. Chapter 2 describes a macroscale approach, wherein commercially available conductive threads are wrapped with a polymer film to enable a touch-sensing fabric using contact electrification. Next, Chapter 3 describes how conventional fabrics, such as cotton and cotton blends, can be surface-modified using solution chemistry to enable a human-body-motion sensor that operates on triboelectric principles. In comparison, Chapter 4 shows how similar fabrics can be surface-modified using initiated chemical vapor deposition (iCVD) to expand the scope of useable polymers and textiles. Finally, Chapter 5 details a third approach, wherein iCVD is accompanied by minimal solution chemistry to yield ionically conductive textiles relevant for supercapacitor electrolytes.

1.2   The Triboelectric Effect

Before any experimental details are described, it is first necessary to explain the underlying scientific principles on which the devices in this work are based, beginning with the triboelectric effect. The triboelectric effect can be defined as induction of charges on electrodes due to potential differences caused by contact electrification. **Figure 1.1** illustrates this principle using a 2-electrode triboelectric device in vertical contact mode.

When the dielectric layers come into contact, charges accumulate on each surface but in the same plane. A potential difference arises when the dielectric layers are pulled apart, and the respective electrodes become charged to counterbalance the potential change between the dielectric and electrode interface. The induced potential difference in the electrodes then causes current to flow to equilibrate for the charges on the electrodes. *(It should be noted here that the research presented in this work does not seek to address the origins of the charges created during contact electrification due to lack of agreement in the scientific community [17, 18] but rather operates on the fact that contact electrification occurs and can therefore be utilized.)*

Due to the device architecture, triboelectric devices can be thought of as a type
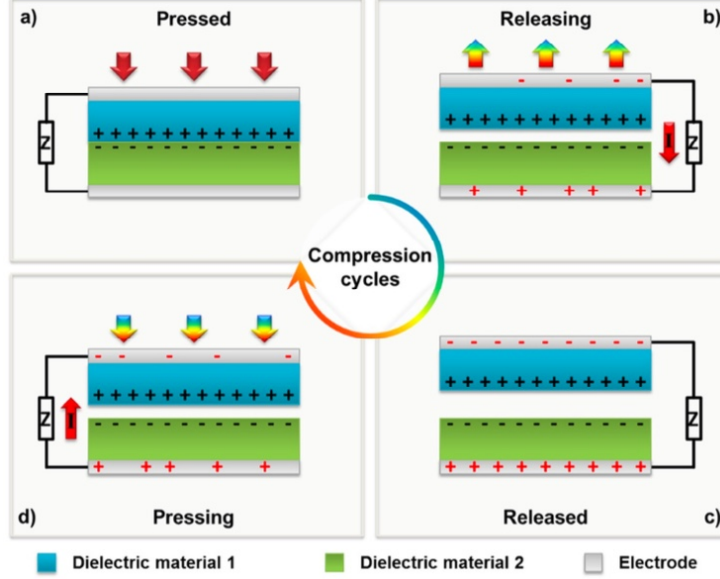
Figure 1.1: Operation of a triboelectric device in vertical contact mode. Image copied from reference [16].

of capacitor in order to mathematically derive the voltage and current outputs. The capacitor in this case consists of two dielectric materials each connected to an electrode, and expressions for voltage and current can be derived from Gauss's Law for electric flux out of a closed surface, as described by Wang et al. [19] and summarized in **Equations 1.1** and **1.2**:

$$V_{oc} = \frac{\sigma x(t)}{\varepsilon_0} \tag{1.1}$$

where σ is the surface charge density on the electrodes, $x(t)$ is the instantaneous distance between dielectric layers and ε_0 is the permittivity of vacuum. Short-circuit current, wherein no voltage is applied, depends on effective thickness (d_0) of the device layers in addition to instantaneous distance between layers and surface charge density:

$$I_{sc} = \frac{\sigma d_0}{(d_0 + x(t))^2}\frac{dx}{dt} \qquad where \ d_0 = \frac{d_1}{\varepsilon_{r1}} + \frac{d_2}{\varepsilon_{r2}} \tag{1.2}$$

Equation 1.2 shows how effective thickness takes into consideration the dielectric constants of each device layer (ε_{r1} and ε_{r2}) as well as their respective thicknesses, assuming the device has two dielectric layers. It should also be noted that I_{sc} is short-circuit current,

which is a measure of a device output sans active area quantification. Throughout this work, short-circuit current density ($J_{sc} = \frac{I_{sc}}{device/area}$) is used to account for the active area of many of the devices for the sake of comparison, as is done with solar cells. Active area is significant because greater device area will result in a greater number of charges created and collected in total compared to smaller devices. However, devices of different sizes can be compared by using J_{sc} values because it normalizes current outputs with respect to device size.

1.2.1 Triboelectric Series

Common dielectric materials have been ranked in their general ability to charge either positively or negatively *after* contact with a different material. This ranking has come about from empirical observations and is presented as a triboelectric series. An example of a triboelectric series with textiles and polymers relevant to this work is shown in **Figure 1.2**.

One thing common to most triboelectric series is that fluoropolymers tend to charge negatively and to a larger magnitude than other materials, whereas cotton tends not to charge quite as positively as nylon, wool, or even the human body (skin).
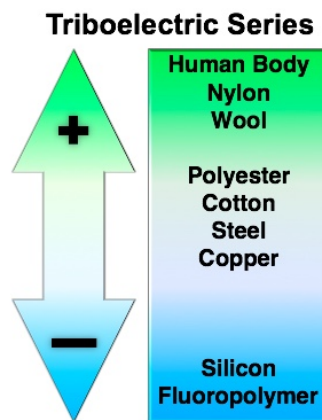
Figure 1.2: Triboelectric Series. Extracted from reference 21.

One thing that is significant to notice is that the majority of commercially-made textiles are dielectric, along with a large number of common polymers. These range from naturally sourced materials like wool, cotton, and rayon, to synthetics such as polyester,

4

silicones, and nylon. Those relevant to this work have been included in the triboelectric series shown in **Figure 1.2**, which was compiled from various sources. [20]

CHAPTER 2

WEAVING CONVENTIONAL MATERIALS INTO A FABRIC FOR TRIBOELECTRIC INTERACTIVE TOUCH SENSORS

2.1 Introduction

Touch sensitive electronic devices serve as the primary user interface for a plethora of current technologies, such as portable computers, e-readers, smart phones, touch pad controls, and interactive display screens. [21, 22] In recent years there have also been significant efforts to create tactile sensing mechanisms that are portable and wearable for use as interfaces in smart clothing and as electronic skin. [23–25] Two main types of touch sensing surfaces are in use in these technologies: resistive touch sensors and capacitive touch sensors. [21, 26] Resistive touch sensors are composed of two conductive sheets arranged face-to-face and physically separated by a micron-length air gap. When a user touches this device, the two conductive sheets are physically brought into contact with each other due to the force associated with the touch interaction, and an electrical signal is recorded and processed by a relevant operating system. Capacitive touch screens are comprised of a single insulating substrate, such as glass or poly(ethylene terephthalate), coated with a patterned array of conductive electrodes on one side. A small voltage is applied across this electrode array, creating a uniform electric field across the opposite, uncoated surface of the insulating substrate. When a user touches this uncoated side, a capacitor is dynamically formed across the electrode-insulator-finger arrangement, since human skin is conductive. The dynamic change in device capacitance is then registered by a controller.

While selected flexible, touch-sensitive device architectures are known, [27, 28] translating these devices to fiber-based substrates is not straightforward. Selected touch-responsive textiles have been previously reported [22, 29–31] that produce a resistance change when an exposed conductive thread comes into direct contact with human skin.

6

However, this method of operation fails when the users' skin or the surface of the touch sensor is dirty, oily, or wet, preventing practical use of textile-based touch sensors in real-world scenarios.

Recently there has been increased scientific interest in triboelectric generators (TEGs) for their ability to convert small force inputs into an electrical (voltage and current) output. Because these devices operate by detecting surface potential changes created upon contact and release of dissimilar surfaces (due to either the triboelectric effect or contact electrification), simple adjustments of device architecture can provide a wide range of functional technologies. [32–34] In this chapter, the triboelectric effect (or, similarly, the contact electrification effect) is used to transduce touch events into an electrical signal using a woven textile composed of fluoropolymer-wrapped [35] conductive fibers. The fluoropolymer wrapping prevents contaminant buildup on the textile surface and also electrically insulates the conductive thread core. Triboelectric textile touch sensors are found to be advantageously insensitive to common environmental variables, indicating promising use as touch interfaces in smart clothing, electronic skin, or furniture and interior design.

2.2   Applications That Make Use of the Triboelectric Effect

Although the triboelectric effect has been observed for centuries, interest therein has recently resurged as a means of harvesting energy from various types of motion, big or small. For example, contact-sliding mode triboelectric nanogenerators (TENGs) have been proposed to harvest additional energy from the spinning of wind turbines, [36] and freestanding triboelectric-layer mode has been proposed as a means of harvesting energy from vibrational motions of air flow. [37]

The key feature of these devices is that they are able to scavenge energy from very minute contact events, and this makes them ideal for use as tactile sensors. [38] This type of application requires single-electrode triboelectric configuration, an example of which is illustrated in **Figure 2.1**.

As shown, the human body acts both as a reference electrode and a surface charging material in the single-electrode configuration. When the skin touches the insulating layer,

7
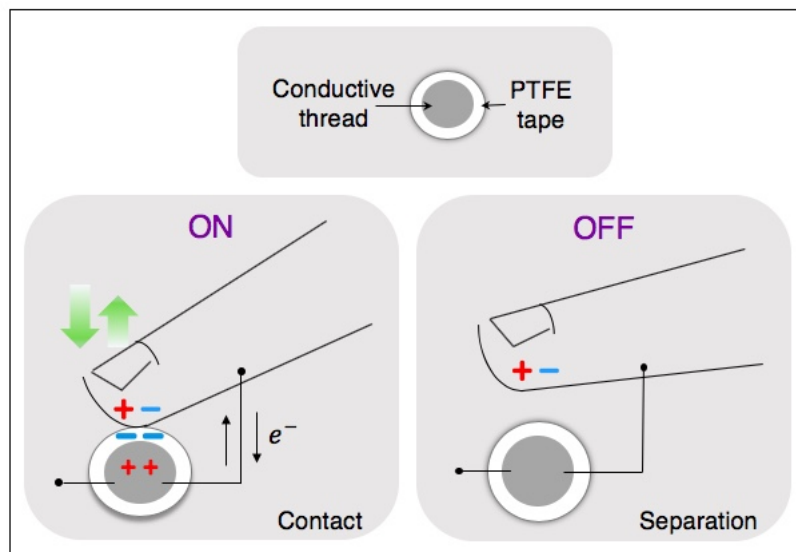
Figure 2.1: Operation of a Single-Electrode Device. Inferred from operation and literature. [39]

poly(tetrafluoroethylene) (PTFE) tape in **Figure 2.1**, charges are built up on the surface of the skin and the PTFE. Upon separating the skin from the dielectric layer, compensation charges are induced on the conductive material and collected at open circuit. Thus, unlike capacitive- or resistive-type tactile sensors, tribo sensors do not require any current input to operate. It should also be noted that the current that results from contact/separation events is alternating (AC), wherein charges are shuttled back and forth between the body and the electrode to compensate for charge buildup on the electrode or skin, respectively. [39, 40]

2.3 Device Design Considerations for Optimal Short-Circuit Current Output

2.3.1 Thread and tape properties (conductivity, thickness, workability)

In order to fabricate a basic tribo device, there must be a conductive layer component and a dielectric layer component. For the sake of maximizing surface contact over a given area, threads were identified as a desirable structure due to surface roughness on multiple scale levels, which results in huge surface areas compared to flat, smooth, polymeric surfaces. Conductive thread was chosen in lieu of conductive wires for the sake of device flexibility. In addition, PTFE tape (purchased from Grainger Industrial Supply)

8

Table 2.1: Properties of Selected Conductive Threads

Material	Vendor	Reported Resistance (Ω/cm)	Diameter (µm)	Notes
Silver Nylon Thread	Syscom (Agsis)	0.200	80	Too thin, expensive
Stainless Steel Yarn	Adafruit	0.394	300	Sticky/not slippery, limp, tears easily
Stainless Steel Thread	Adafruit	0.512	200	High tensile strength, moderately slippery, stiff
Silver Nylon Thread	LessEMF	20-30	140	Kinked, stiff
Silver Nylon Thread (bulk)	LessEMF	100	180	Most like nylon thread

was selected as the dielectric material because it could be easily wrapped around thread via dry self-adhesion, and fluoropolymers are known to charge negatively and to a higher magnitude than most other materials due to fluorine having the highest electronegativity of all elements. [20, 41]

In terms of selecting a conductive thread to serve as the electrode, many options are commercially available. However, they are not all equivalent and cannot be selected solely on conductivity/resistivity, which affects current flow in a circuit in accordance with Ohm's Law (I=V/R, where I is current, V is voltage, and R is resistance). Other factors, including differences in thickness and strength of the threads greatly determine their ease-of-use but in turn alter the device output and in many cases the resulting device architecture and flexibility. **Table 2.1** summarizes the threads that were considered and tested for use in this work.

As described in the "Notes" column of **Table 2.1**, metal and metal-plated threads such as stainless steel and silver nylon, respectively, are unlike conventional nylon, cotton, or polyester threads because in general they are stiff with high tensile strength, making them difficult to wrap with PTFE tape, to knit and weave, or both. For example, although the stainless steel yarn exhibits the best conductivity and the greatest surface area, both

desirable for triboelectric devices, its tendency to stick to itself and ease of tearing made it nearly impossible to work with for weaving or knitting. In addition, the fuzziness of the thread that is a result of stray fiber strands interfered with the PTFE's self-adhesive properties (van der Waal forces), making it difficult to fully encase the thread without it unwinding the tape before weaving or knitting. Conversely, the bulk silver nylon thread, while easiest to work with, was too thin and electrically resistive for the purposes of this work. The thinness made the bulk silver nylon thread easily slide out of the tape encasing, causing electrical shorts in some devices, and the resistivity resulted in very low triboelectric signal. Therefore, given the ease with which the stainless steel and silver nylon threads could be wrapped and their relatively low resistance, the majority of devices were made using either the stainless steel thread (0.512 Ω/cm, 200 μ/m diameter) or the silver nylon thread (20-30 Ω/cm, 140 μm diameter).

In addition to thread workability, the PTFE tape thickness must also be considered, not only for the sake of triboelectric output (dielectric layer thickness in **Eq 1.2** shows thinner dielectrics are optimal), but also to prevent the threads from breaking through the tape during the wrapping and weaving processes and causing circuit shorting, as was observed in some cases. **Figure 2.2** shows how the low-density PTFE tape, with specific gravity (sg), i.e. density, on the order of 0.35 - 0.5 and thickness of 88.9 nm, can be easily over-stretched and broken by a single stainless steel thread in comparison with the thinner, weaker silver nylon threads, two of which together do not appear to strain the tape. Medium-density PTFE tape (sg $\approx$ 0.7-0.8, thickness = 102 μm) was therefore used for some of the stainless-steel-thread-based devices.

2.3.2   Effects of Weave Density on Current Output

A number of devices were constructed by hand in order to gain insight into the effects of weave density and wrapped thread density (number of threads per strand) on device outputs. This section focuses on the weave density. **Fig 2.3** illustrates the device construction process, wherein the conductive thread or threads are wrapped with PTFE tape, then woven. Two stainless steel thread-based devices were woven such that only one

Figure 2.2: Thread(s) wrapped in low-density PTFE tape. Images show woven devices.

warp or one weft strand was left bare at one end for use as an electrode connection (Version 1.0). All other devices were made such that the warp threads were individual strands woven together by a single weft strand (Version 2.0). The warp threads were then left bare at one end and bundled for use as the device's electrode.

As indicated in Section 2.2.1, the strand thickness and therein device density can be increased by choosing medium-density over low-density PTFE tape. Device density can also be increased to a small extent by bundling multiple threads in one wrapping. Furthermore, the closer the strands are pushed together when weaving, the denser the resulting device will be in terms of amount of material per unit area. To gain insight on how device density affects the electrical outputs, short-circuit current density (short circuit current per unit area of the device) was compared among four differently-configured devices. Optical images indicating the electrical connections (either one thread for V1.0 or bundled-and-alligator-clipped threads for V2.0) are accompanied by a table of device data in **Figure 2.4**. Devices A and C were made using a single stainless-steel thread wrapped in low-density PTFE tape. Devices B and D were made using two stainless-steel threads wrapped in medium-density PTFE tape. All short-circuit current outputs in this work were measured using a Wavenow potentiostat with the chronoamperometry experiment set to zero volts (short-circuit current conditions). Current output is generally the limiting metric for all triboelectric devices, which otherwise generate remarkably high open-circuit
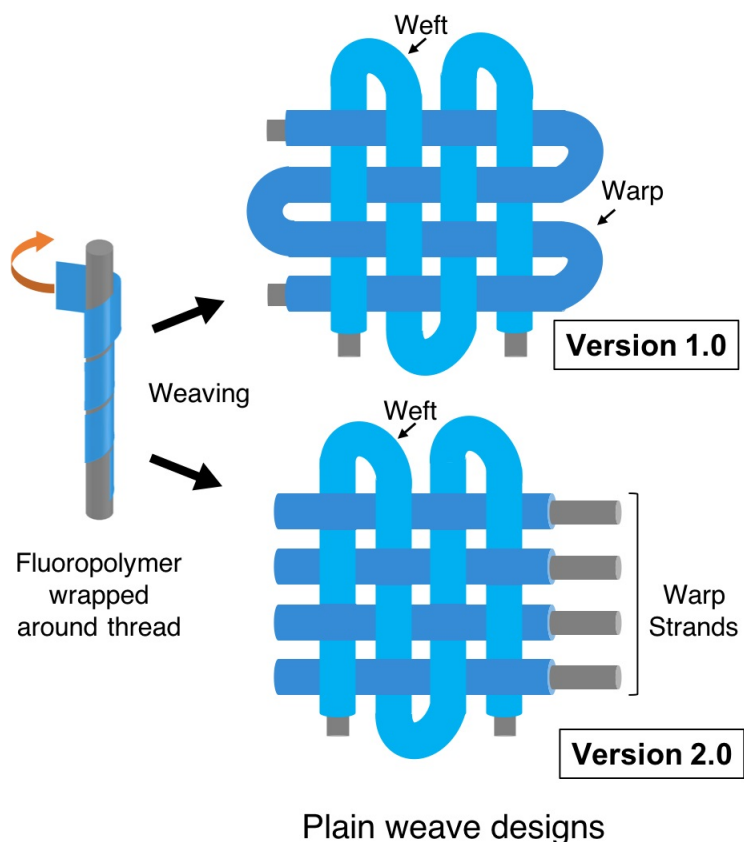
Figure 2.3: Device construction with different versions of the plain weave design.

voltages. [32–34] Therefore, in this work, the current output of the textile is primarily used as the distinguishing metric with which to identify touch events under various conditions.

It should first be noted that this experiment could have been executed in such a way as to better isolate the effects of the different parameters on the devices. However, multiple devices were made in a short period of time, then grouped for analysis, which prevented complete isolation and the drawing of significant conclusions. Nonetheless, some insights could be gathered.

From **Figure 2.5**, there are two possible insights to glean. The first is that weave version 2.0 (devices C and D) yields higher output in general than version 1.0 (devices A and B). This is likely due to connecting the strands in parallel (all bundled using one alligator clip), which provides more pathways and shorter pathways for charges to be collected. On the other hand, weave version 1.0 devices (A and B) are connected to the detector via only one or two warp threads, respectively, which can be thought of as a series connection of the
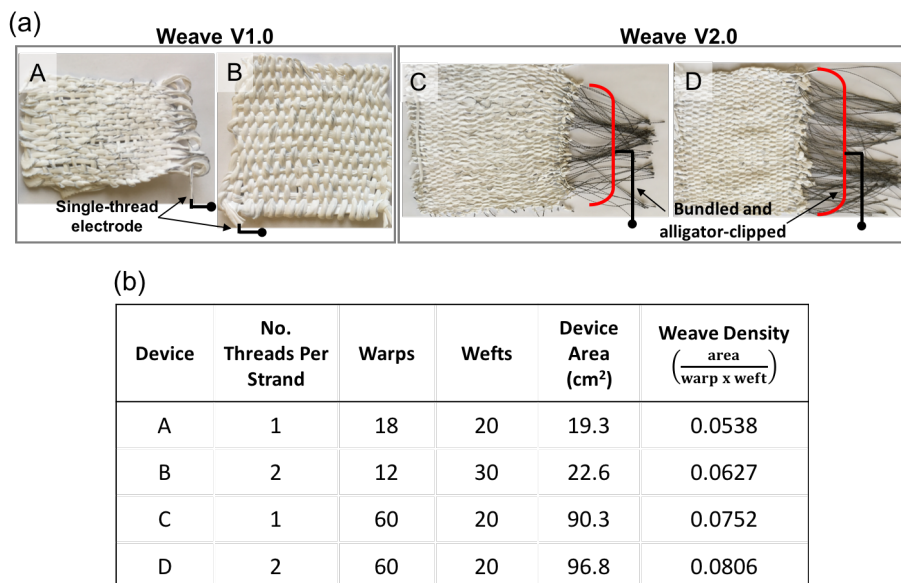
Figure 2.4: Device weaves and data.**(a)** Optical images of the devices and their respective weave version from **Fig 2.3**. **(b)** Device data table.
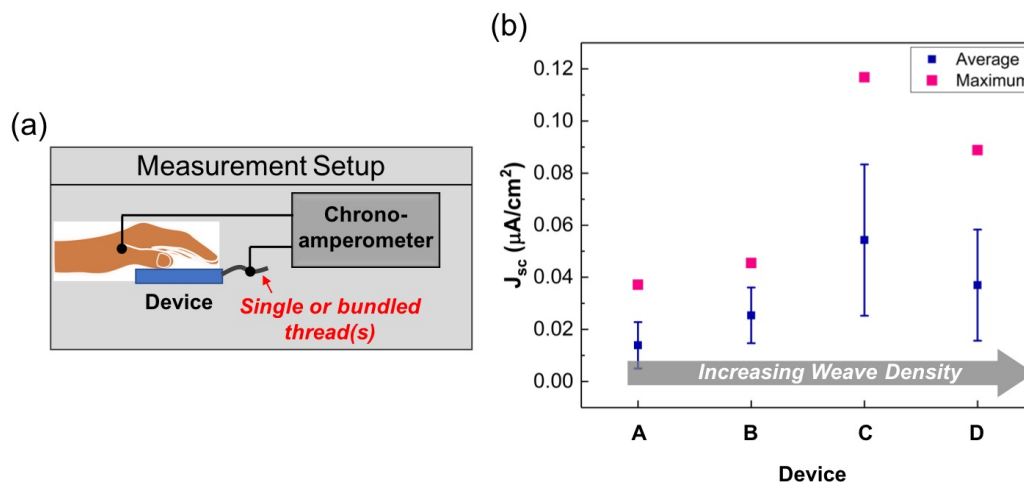
Figure 2.5: Weave density tests.**(a)** Measurement setup illustration. **(b)** Short-circuit current density peak height averages and maxima. Error bars indicate standard deviation of signal outputs over a 20 s period of repeated tapping.

circuit. With only this one electrode connection point, charges built up on the weft threads were not collected. For this reason, the version 2.0 design was adopted in later experiments, and testing shows that per unit area, the version 2.0 weave results in higher current outputs per unit area, as expected.

The second insight from **Figure 2.5** could be that there is an optimal weave density beyond which electrical performance does not necessarily benefit. The optimal configuration

13

for the tested devices is that of device C, which consists of a single stainless steel thread wrapped in low-density fluoropolymer tape and woven in the version 2.0 method. There can be two reasons for device C having the greatest current output per unit area of device: (1) Charge collection is optimized in accordance with **Eqn 1.2** because the dielectric layer is thin, and (2) Wrapping two threads into one strand may create a shielding effect and prevent contact between the dielectric layer and electrode threads or between electrode threads and the alligator clip that serves as the connection to the chronoamperometer. According to literature [39] the number of threads wrapped together should make little difference on the device output. This is true if we compare devices A and B, the electrode threads of which could be connected to the detector with no loss of direct connection to the alligator clip. Although this points toward the electrode-to-detector shielding rather than one bundled thread shielding another from the dielectric layer, the effects of PTFE tape thickness were not tested in isolation and could be part of the reason device D showed lower J_{sc} than device C. Again, this data is inconclusive amongst all devices because tape thickness also increased from devices A to B, as did Jsc, opposite of the relationship observed between devices C and D. Overall, too many variants between devices leads to lack of evidence for any real trends.

2.3.3 Ag-nylon Woven with 1, 2, and 4 Threads

To deconvolute the effects of tape thickness and number of threads wrapped in fluoropolymer tape per strand, woven devices in the version 2.0 weave configuration with similar size were constructed using only low-density tape and silver nylon thread (20-30 Ω/cm). The number of threads per strand remained uniform throughout a single device but varied from one device to the next, producing one device with a single thread per strand, one with two, and one with four threads per strand. Each device consisted of 60 warp and 20 weft strands. The maximum and average value of short-circuit current density peak heights are shown in **Figure 2.6**.

From the graph in **Figure 2.6**, it is evident that increasing the number of threads per strand lowers the short-circuit current density output of the triboelectric devices, al-
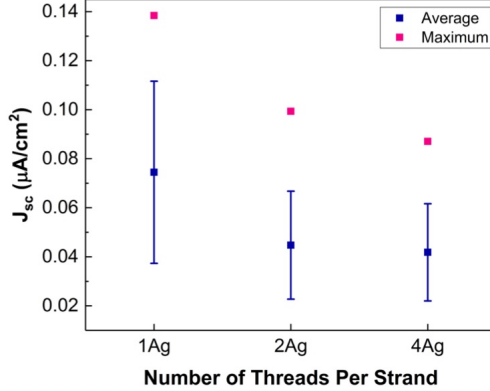
Figure 2.6: Silver nylon thread density tests. Short-circuit current density peak averages and maxima for silver-plated nylon thread-based devices with increasing thread density. Error bars represent standard deviation among measurements made within a 20-second period of repeated tapping.

though not to a significant degree. The averages differ between devices by only hundredths of microamps per square centimeter, as do the maximum values. However, this data could be used to support data from the stainless steel devices woven in the version 2.0 configuration (devices C and D) in Section 1.2.2. The decrease in outputs observed in version 2.0 devices made with either silver nylon or stainless-steel threads may be an indication that bundling is not ideal if the alligator clips (detector) are (is) not directly touching all threads. A testing setup that connects each conductive thread individually to the detector in parallel configuration could better clarify this concept.

Seeking other insights from these device variations, select data from **Figures 2.5** and **2.6** were combined and are presented in **Figure 2.7**. Two observations can be made here. Comparing the single-thread devices, we see there is little difference in both the maximum and average J_{sc} values whether the device is made with stainless-steel thread (0.512 Ω/cm resistance) or silver nylon thread (20-30 Ω/cm resistance). This may suggest that either resistance of the threads has no significant effect on device performance, or there is a threshold resistance beyond which device performance suffers. The latter may be true considering devices made with the bulk silver nylon thread (100 Ω/cm) yielded undetectable outputs.

If we use the assumption that there is no difference in current output between devices made with stainless-steel vs silver nylon thread, it can also be inferred from **Fig-**
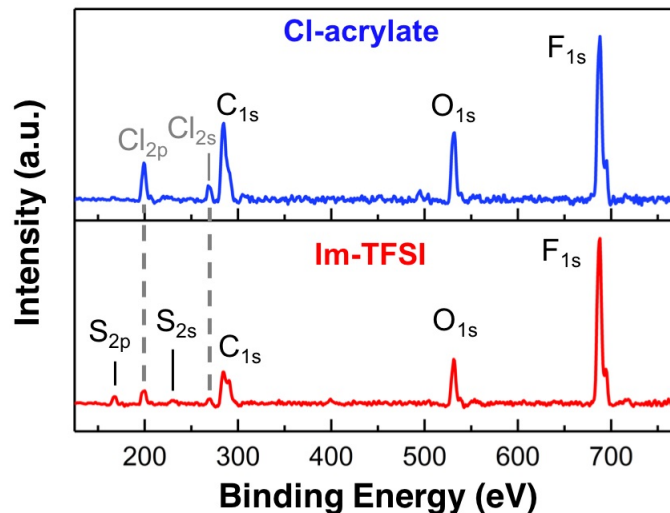
Figure 2.7: Comparison of thread type and fluoropolymer tape thickness for devices of similar sizes. "SS" is stainless steel thread, and "Ag" is silver-plated nylon thread. Error bars represent standard deviation among measurements made within a 20-second period of repeated tapping.

ure 2.7 that fluoropolymer tape thickness has negligible effect on device performance, as evidenced by the similar maximum and average J_{sc} values of the 2-thread silver nylon device, which was wrapped with low-density tape, and the 2-thread stainless steel device, which was wrapped with medium-density tape. However, the extent to which bundling the threads effects the devices is not accounted for here, so this conclusion cannot be made with certainty.

2.4   A Plausible Touch-Sensing Device

In the previous two sections, the tactile-sensing fabrics were optimized. Here it is described how the optimized fabric can be configured to make a viable device.

Each warp thread in the woven textile touch sensor can, in theory, be connected to an independent sensing channel of a controller, which will only register an electrical signal when a user touches the part of the textile containing this thread. For this study, an oscilloscope with three independent channels is used and, therefore, the bare ends of the warp threads of the textile are portioned and bundled together to form three spatially-distinct (lengthwise) channels, labelled Region 1, 2, or 3 (**Figure 2.8**). Each of three channels operates independently and only manifests an electrical output when the corresponding region

of the textile is touched. Therefore, this textile touch sensor automatically demonstrates spatial resolution concomitant with the weave density used to create the device. Further, when a finger is swiped across a large region of the textile, the shape of the electrical output is notably different and multiple channels record the dragging motion.
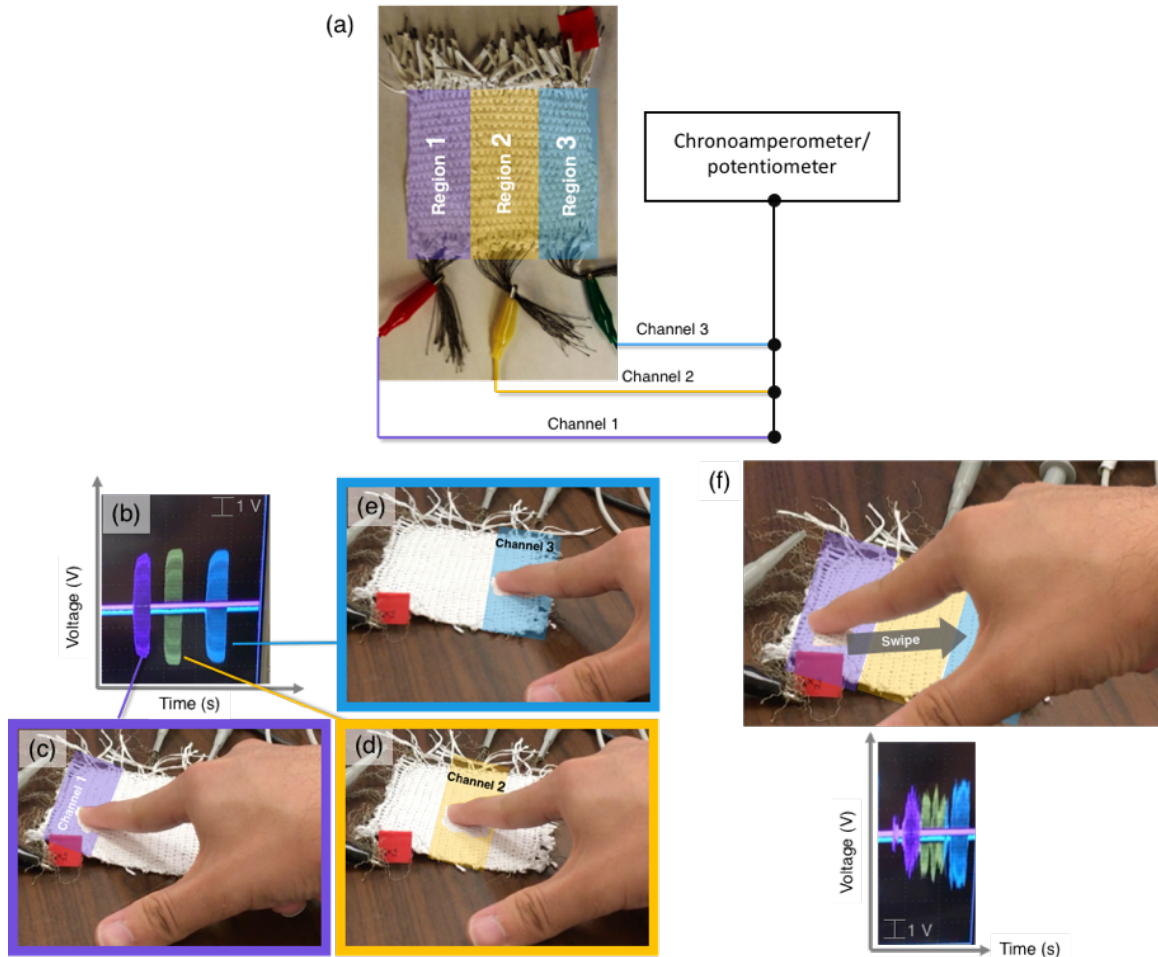
Figure 2.8: Tactile channels.**(a)** Circuit diagram for testing woven textile touch sensors. Conductive threads from each string are bundled and connected to the potentiometer/chronoamperometer, segmenting the device into separate readout channels indicated by the different colored areas. **(b)** Voltage output with a 500 GW load resistance from three different sensing channels (purple, yellow, blue) when the corresponding spatial regions of the textile sensor (highlighted) are touched **(c-e)**. **(f)** Voltage output with a 500 GW load resistance when a finger is swiped across the length of the textile touch sensor. Output shows groups of signals from momentarily holding finger on device.

In testing the different channels, it became obvious that different gestural motions result in varied electrical output of the fabric. For contact electrification it is a general rule that smaller applied forces result in a smaller contact area and therefore smaller electrical output than for greater applied forces. This rule was confirmed by the short-circuit current

output presented in **Figure 2.9**. Events with smaller applied force, such as swiping the hand across the device or touching softly, resulted in smaller short-circuit current outputs than harder slaps or pounds. Nonetheless, the lighter touches still output the same magnitude of current on the order of a few microamps, which is sufficiently detectable for an interactive touch application.
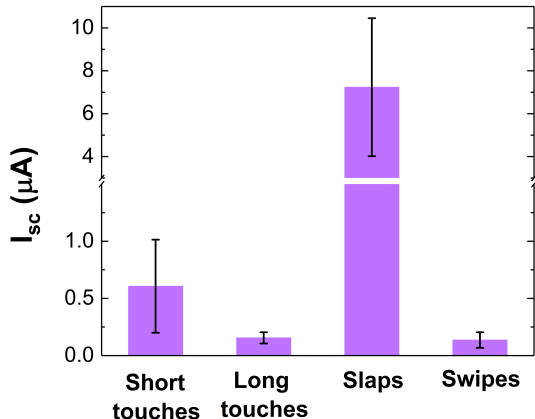
Figure 2.9: Current output under short circuit conditions for different gestures. Short touches and slaps lasted approximately 0.5 seconds, while long touches lasted approximately 1 to 1.5 seconds, and swipes lasted approximately 2 seconds. Error bars represent standard deviation among measurements made within a 20-second period of repeated touches.

2.5 Signal Stability Under Different Conditions

Touch sensors are typically operated under dirty, "real-world" conditions where grease, sweat, salt, water and/or other biofilms will accumulate on the surface of the sensor. Therefore, it is necessary to understand how the electrical output of the textile touch sensor is affected by common environmental variables, such as water, sweat, and oil that can be present on the surface of the interactor's skin. In order to assess the performance of the textile touch sensors in humid and sweaty environments, the current output under short circuit conditions are tested in two different ways: by wetting the sample surface and testing with dry hands and by using wet/salty hands to touch a dry sample surface. Furthermore, the sensors are tested using lotion-saturated skin to mimic oily biofilms. All of these testing conditions are explored because the PTFE wrapping effectively protects the conductive

Table 2.2: Summary of Tests of Realistic Conditions

Condition	Details	Effect
Ambient	Dry hands, dry textile surface	Control
D.I. H_2O	Deionized water	Humidity
Tap H_2O	Tap water	Humidity, dirt, particulates
D.I. + salt	40 mM NaCl in deionized water	Humidity, ions
Tap + salt	40 mM NaCl in tap water	Humidity, ions, dirt, particulates
Lotion	Lubriderm daily moisturizer	Grease, oils

thread cores of the textile and prevents salt/biofilm accumulation on the textile surface. In order to mimic the realistic conditions, deionized (D.I.) water was used to test humidity, and tap water was used to test humidity, dirt, and other particles. Furthermore, salt water solutions (40 mmol/L NaCl) were made to mimic sweat [42] and ions in general. Using a spray bottle, each solution was sprayed directly onto the tester's hands or onto the textile before testing, in accordance with the indicated test in **Figure 2.10** below. Finally, lotion was applied amply to the tester's hands to mimic the presence of grease and oils. **Table 2.2** summarizes the tests and their intended mimicked effects.

Minimal changes in the average current output from the textile touch sensor are observed for wet, dry and oily testing conditions **Figure 2.10**. The observed voltage outputs from the textile touch sensor are similarly insensitive to the particular wetness or dirtiness of the surface or of the user's hand, although a globally-lowered voltage output is observed in the presence of excess water or ions, likely because skin-contact-created surface charges are rapidly dissipated into the aqueous or ionic environment. [43] Similarly, wet surfaces and wet/salty hands result in greater standard deviation in the magnitude of the observed current output **(Figure 2.10 b-d)** but the averaged current output value is similar to the average current output when a pristine, dry textile is touched with clean, dry hands.

The two exceptions are the noticeably lower current output generated when the textile touch sensor is touched with a finger dipped into a salt water solution made with tap water or with lotion-saturated skin. Only the current output is affected in both cases and the
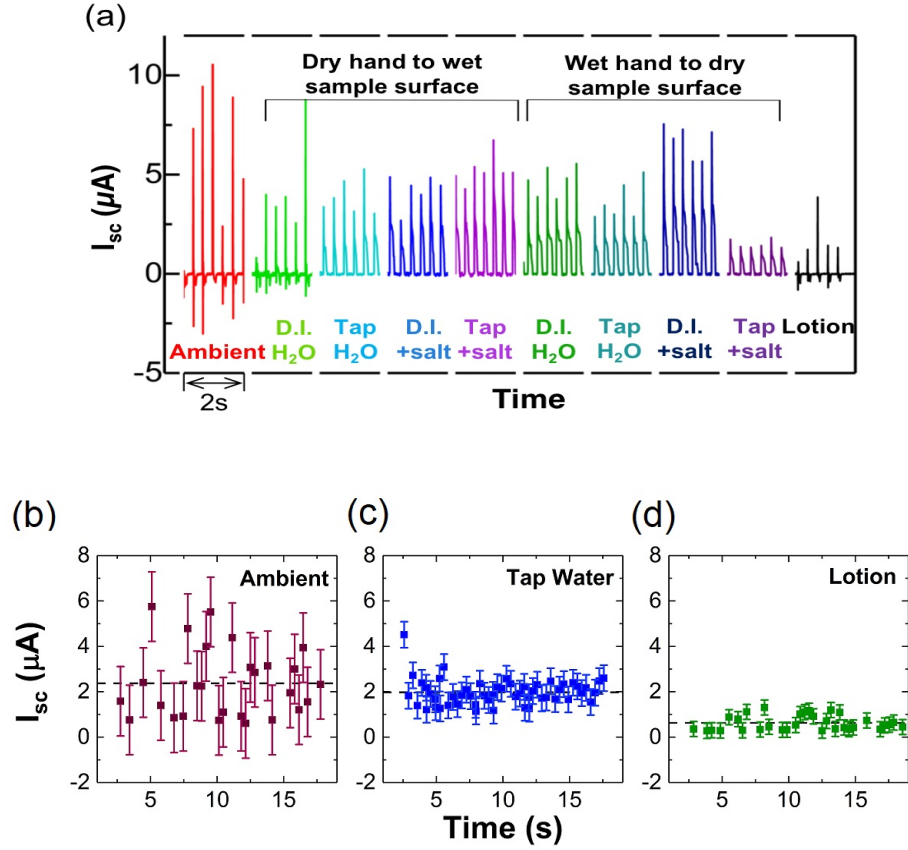
Figure 2.10: Testing of devices in varied environments.(a) Short-circuit current of device by environment. (b-d) Averages with standard deviations of select tests from top.

voltage outputs remain unchanged compared to other testing conditions. Further, fingers dipped in brine made with distilled water do not yield a lowered current output. We posit that these tap water and lotion outliers likely arise due to mechanical disruptions—the salty tap water and lotion make the surface of the user's skin especially sticky and subsequent touch interactions jostle the electrical connections attached to the textile touch sensor. This likely causes an increase in thread resistance that manifests as a lowered current output.

To further test the extent to which oils affect the current output of the tactile sensor fabrics, experiments were done before, during, and after lotion was applied to the sensor surface and removed by wiping with a cleaner (either commercial cleaning product or isopropanol). Both the devices, either made with silver-plated nylon thread or stainless steel thread, showed a decrease in current output by approximately one order of magnitude while excessive amounts of lotion were present but returned to normal functionality after

the lotion was cleaned from the device surface. These results suggest that the oils interfere slightly with the triboelectric effect, but not enough to prevent device function. Maximum current output peak values and average current output peak values with standard deviation for these experiments are shown in **Figure 2.11**.

Overall, surface wetness and wet/sweaty fingers do not meaningfully change the current output generated by the textile touch sensor, qualifying this fabric for real-world operability.
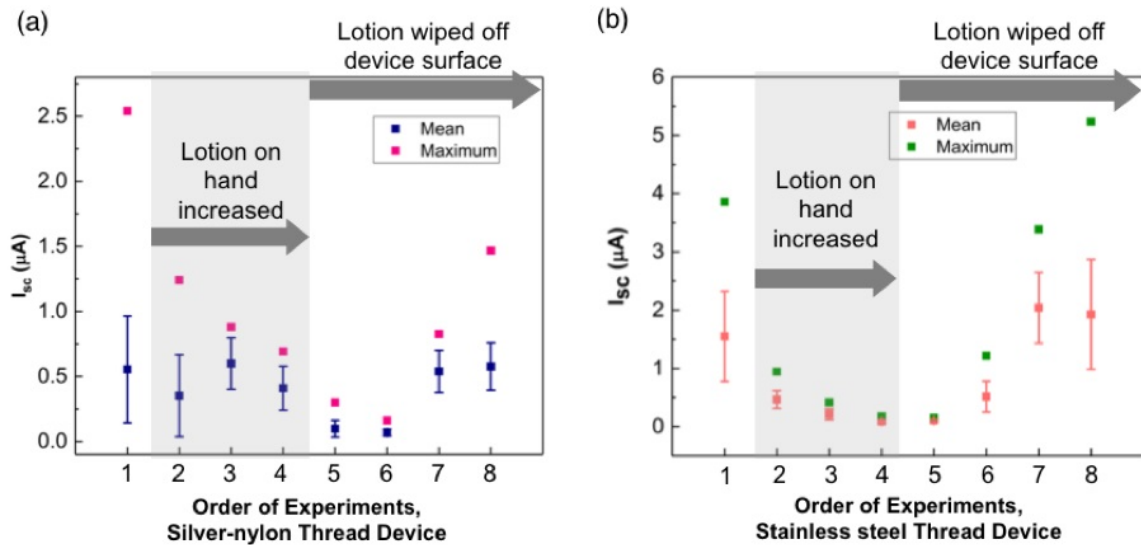
Figure 2.11: Means and deviations of current outputs for different conditions. Maximum and mean (with standard deviation) peak values of current output generated upon repeated contact and separation with excess lotion on the skin surface. **(a)** Shows results for silver-plated nylon thread devices, and **(b)** shows results for stainless steel thread devices. Note the slight difference in y-axis scales.

2.6   Summary

To recap, this chapter shows how threads can be modified on a macro scale and woven together to create a triboelectric tactile-sensing fabric. Multiple iterations of conductive thread and fluoropolymer tape were investigated to determine the optimal fabric architecture, but few conclusions could be drawn due to poor experimental setup that overlapped variables without a clear control device. Still, these experiments were relevant and allowed for the discovery that the stainless steel threads were easiest to work with. The

stainless-steel-thread-based fabrics were therefore tested to determine tactile sensing capabilities under realistic conditions. It was discovered that gestural differences could be identified by the respective changes in current output. In addition, the influence of surface wetness and varying skin surface composition were studied, and the tactile sensor fabric was found to be advantageously insensitive to these environmental variables. The woven textile touch sensors are as flexible as natural fabrics and could foreseeably be implemented as a touchpad controller, as electronic skin, or as part of a health monitor, among other applications.

CHAPTER 3

MODIFYING CONVENTIONAL FABRIC SURFACES USING WET CHEMISTRY

3.1   Introduction

In Chapter 2 it was described how conventional materials can be woven into a tactile-sensing fabric. Although this provides a simple fabrication method, the functional material is limited to fluoropolymer tape, which is highly flexible, insulating, self-adhesive, and in a unique physical form, unlike any other material. This uniqueness severely limits the properties and applications of the fabric.

Nonetheless, fabric itself is understood to have its own contact electrification capability, although natural fabrics significantly less so than synthetics. However, natural fabrics like cotton and linen are made of cellulose, which means there are many hydroxide groups on the material's surface that can easily undergo chemical reactions, especially surface grafting. [44–46] Furthermore, the naturally rough surfaces of textiles are ideal for maximizing contact area in a triboelectric architecture. For these reasons, a method for fabric modification was investigated with the specific goals of maintaining fabric feel and flexibility while creating an electronically-functional textile device.

Using a silane-grafting technique, Chapter 3 thus illustrates how natural fabrics can be tuned on the surface to improve contact electrification for triboelectric devices. Active layer thickness and scalability were investigated, and construction of a triboelectric motion-sensing elbow sleeve gave insight to the applicability of the grafting technique used in a realistic setting.

3.2   Grafting Silanes to Cotton Fabrics

To recall the triboelectric series discussed in Chapter 1, it is understood that cotton, wool, and nylon tend to charge toward the positive end of the spectrum. Although

these materials could be charged via contact with another cotton, wool, or nylon swatch, respectively, charges can be maximized by using materials from opposite ends of the tribo series. [35] However, that limits devices made with commercial fabrics to combinations of nylons and polyesters and excludes natural fibers that are most comfortable to wear, the most obvious example being cotton.

Therefore, to achieve truly wearable tribo-active fabrics with maximum device output, methods to functionalize the surfaces of cotton fabrics were investigated, starting with a solution process.

Natural fabrics and threads are relatively easy to functionalize in solution due to their cellulose composition. In particular, cotton, after scouring and bleaching for industrial use, contains 99% cellulose, which is known for its amenability to chemical grafting. [47,48] Taking advantage of the many available hydroxyl groups on the cellulosic fabric surface, a simple silane grafting technique [49] was carried out to yield fluorine-rich surfaces. Although multiple studies have been done that use silanes to modify textiles for various properties, [50–54] this is the first experiment to use this chemistry in fabricating triboelectric-active textiles. **Figure 3.1** depicts the functionalization chemistry, which occurs in four steps, according to known formation of self-assembled monolayers on hydroxylated silicon wafers: 1) Physisorption, 2) Hydrolysis, 3) Covalent grafting, and finally 4) In-plane reticulation.
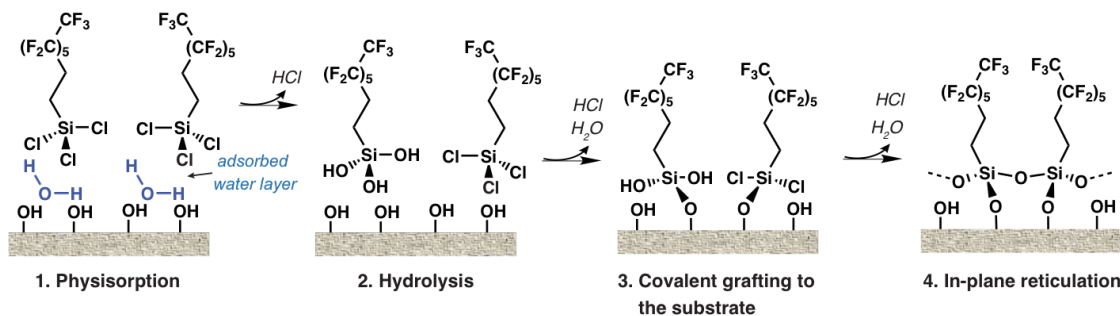
Figure 3.1: Silanization on cotton. Process shown using trichloro(1H,1H,2H,2H-perfluorooctyl)silane.

During Physisorption, the silane moiety is physically absorbed onto the fabric

Table 3.1: Silane grafting solutions.

Ref. Name	Solute	Solvent	Vol% (solute/solvent)	Structure
Si-F	trichloro(1H,1H,2H,2H-perfluorooctyl)silane	hexanes	1	Cl−Si(Cl)(Cl)−$CF_3(CF_2)_5CH_2CH_2$
Si-NH$_2$	(3-aminopropyl)trimethoxysilane	isopropanol	10	H_3CO−Si(OCH$_3$)(OCH$_3$)−$\sim\sim$NH$_2$

surface. Next, hydrolysis occurs, replacing the Si-Cl bonds with Si-OH. Once the silane moiety is hydrated, it can covalently bond to the hydroxyl groups on the fabric surface, self-assembling such that the attached fluorocarbon chains are aligned. With time, the proximity of adsorbed silane moieties causes condensation reactions with neighboring silanes, leaving a polymer grafted to the fabric surface.

For silane grafting to cotton and cotton blend fabrics, the cotton swatches (100% cotton purchased from Dharma Trading Co.) were pre-washed by sonicating in deionized water for 10 minutes, then rinsed with isopropanol and air-dried before soaking in the grafting solution for 25 minutes. The silane moieties and their respective concentrations in the given solvents are reported in **Table 3.1**. Confirmation of successful functionalization was done by triboelectric output in comparison to pristine (unfunctionalized) fabrics, by X-ray photoelectron spectroscopy (XPS), and by spraying water on the surface of the Si-F coatings, since they are well-known for their hydrophobic character. [55, 56] Experimental methods for triboelectric tests are explained in the following section.

The XPS data in **Figure 3.2** indicates the presence of fluorine on the Si-F cotton surface, but not on the pristine cotton surface, as expected. This is shown by the F1s peak (absent in pristine cotton, but present in the Si-F cotton), and in the splitting of the C1s peak in the Si-F spectrum. The C1s peak is shifted to a higher binding energy, as indicated in the inset of **Fig 3.2**, and the second C1s peak appears that is likely due to the fluorinated carbons in the silane molecule.
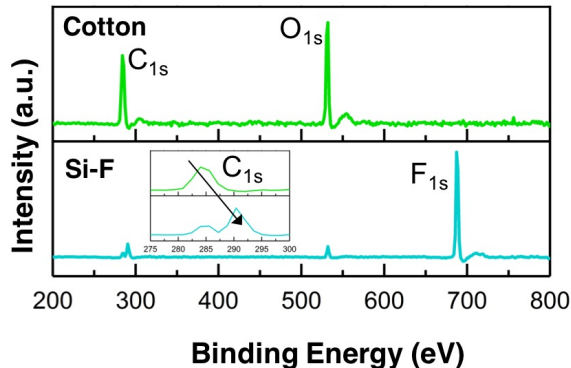
Figure 3.2: XPS data for pristine cotton (green) and silane-grafted fluoropolymer cotton (blue).

3.3 Triboelectric Outputs of Cotton Fabrics Post-Silanization

For the sake of the applications described in later sections of this chapter, the cotton fabrics were analyzed with respect to electrical (short-circuit current and open-circuit voltage) outputs using the vertical contact triboelectric mode described in Chapter 1 and reiterated in **Figure 3.3** below. Each 2 inch x 2 inch (25.8 cm^2) coated textile was sewn to a copper-polyester fabric (LessEMF; thickness 0.08mm, resistivity 0.05 Ω/square) electrode with cotton thread on the contacting side and conductive stainless steel thread on the electrode side that served as electrical connection "wires" from the device to the Wavenow potentiostat. Each half of the device was sewn using five conductive threads in parallel spaced approximately 1 cm apart.

The device layers are shown in **Figure 3.3** along with outputs comparing solution-functionalized cotton signals to those of pristine or unfunctionalized cotton. The blue-colored fabric in **Figure 3.3** represents commercially-purchased nylon, and the tan-colored fabric represents the Si-F functionalized cotton species. As shown, these devices output approximately 10 volts at open circuit and a few microamps per square centimeter under short-circuit conditions. In comparison, the unfunctionalized cotton devices only output fewer than 2V and 0.5 μA/cm^2, respectively. It can be inferred that the fluorinated cotton surface is the reason for the approximate five-fold increase.
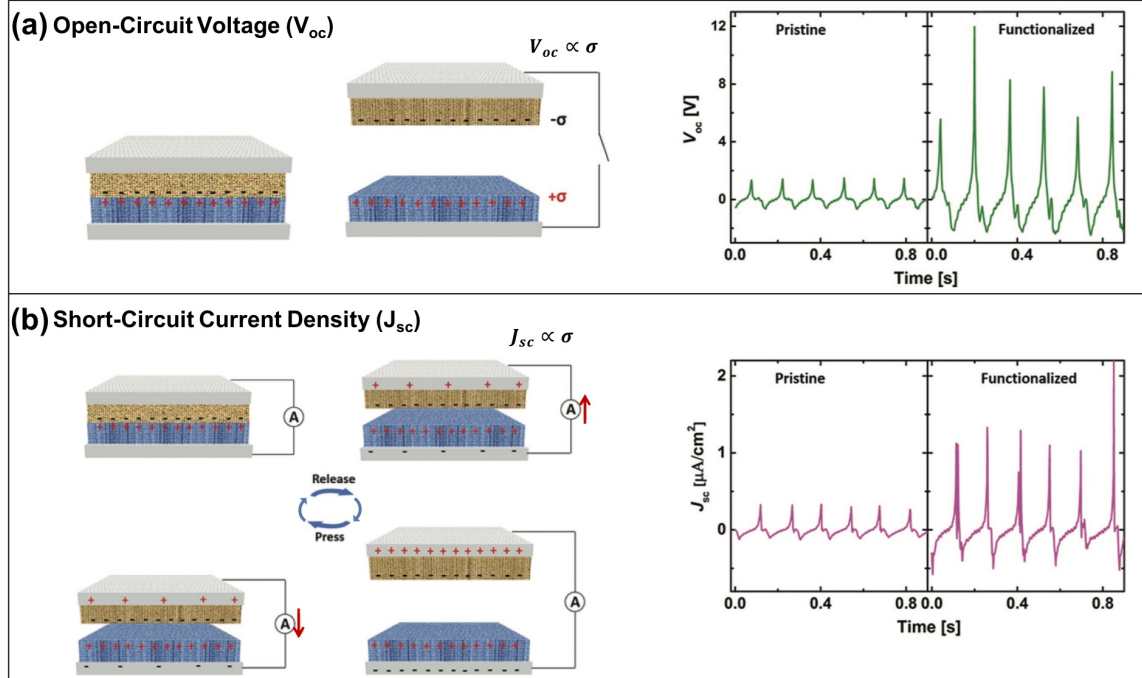
Figure 3.3: Vertical Contact Mode in a Triboelectric Textile Device.

3.4 Effects of Cotton Layer Thickness on Triboelectric Output

Although the outputs for fabric devices were increased by surface modification, they were much less than literature values reported for polymer-based triboelectric devices. [39,57,58] To explain this observation, it was posited that the dielectric materials' thickness may be preventing proper current induction, in accordance with **Equation 1.2** in Chapter 1 of this work. Therefore, devices with thinner (lighter weight) functionalized layers were investigated. All lightweight cotton materials used in this study were 100% cotton from Dharma Trading Co. For each device, one 25.8 cm^2 piece of the cotton was functionalized with Si-NH$_2$ and another with Si-F (**Table 3.1**) to serve as the positive and negative charging dielectric layers, respectively. To each layer was sewn a copper-plated polyester electrode fabric using stainless steel conductive thread, as described previously. **Figure 3.4** below shows the short-circuit current and short-circuit current density of each device, along with the weights of the cotton fabrics before surface grafting.

From **Fig 3.4 (a)**, the current outputs of the devices can be directly compared.

27
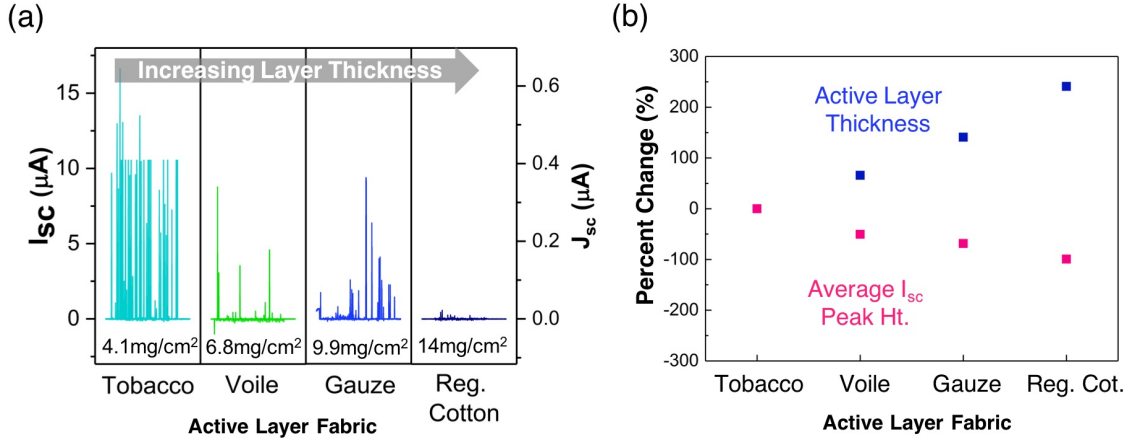
Figure 3.4: Thin cotton fabric triboelectric device outputs. **(a)** Short-circuit current (I_{sc}) and short-circuit current density (J_{sc}). **(b)** Percent change in active thickness (blue) and average I_{sc} peak height (pink) relative to tobacco cloth.

Although the maximum peak height for gauze is slightly greater than that for voile, a clear trend in the average values is presented in **Fig 3.4 (b)**. Here the data was analyzed relative to the values observed for the tobacco-cotton-based device. There is an obvious decrease in current output with increasing cotton fabric thickness, as predicted. This trend is likely due to the fact that as the distance from dielectric surface to electrode surface increases, the compensating charge on the electrodes is lessened, which in turn reduces the induced current.

3.5 Device Scaling

As discussed in Chapter 1, significant efforts have been put forth to create triboelectric devices for the sake of energy harvesting. With respect to human body motions, the pressure exerted from walking on a triboelectric surface could result in significant voltage generation. [59] While many shoe insert designs and triboelectric floors have been proposed to harvest energy from foot traffic or walking, [60–63] few studies have been done with respect to a triboelectric carpet. However, a tribo carpet could easily be achieved using the silane grafting method described in the previous section of this work.

Because all of the devices described thus far have been significantly small in comparison to the size of a small 3'x5' rug, the effects of scaling device size on current output

were first investigated. Three different devices were constructed for comparison, each having a triple-layer structure similar to that shown in **Figure 3.5**. Here the Si-NH$_2$ functionalized cotton layers act as the positive charging surfaces, and the kapton (polyimide) tape as the negative charging surface. The Si-NH$_2$ cotton layers were sewn to the copper-plated polyester layers with conductive stainless steel thread, which served as electrical wires in connecting the device to the chronoamperometer/potentiostat For the kapton tape - covered copper-polyester layer, the copper-polyester fabric served as the direct connection to the chronoamperometer/potentiostat. Three separate devices were made with areas of 2 in. x 2 in. (25.8 cm^2), 6 in. x 6 in. (232.3 cm^2) and 12 in. x 12 in. (929.0 cm^2).
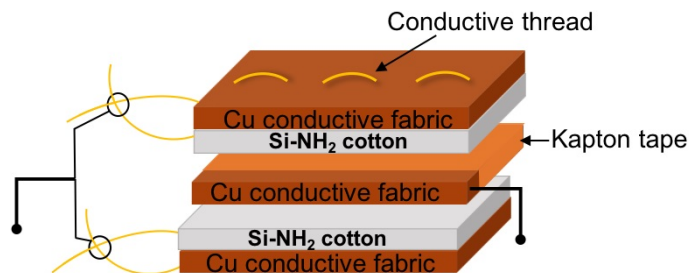
Figure 3.5: Triple-layer device structure.

To compare the short-circuit current density outputs, peak heights were averaged and shown with the maximum peak height values in **Figure 3.6**.
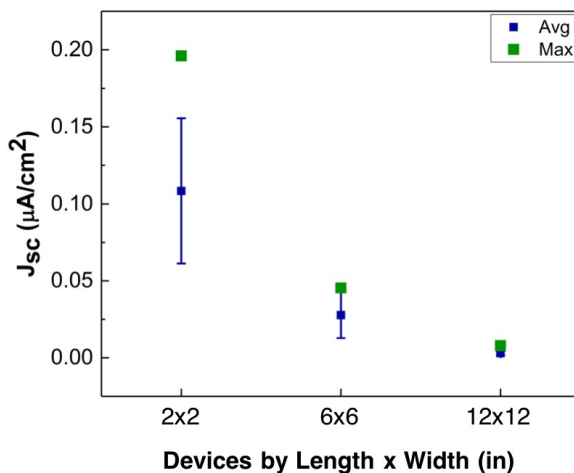
Figure 3.6: Devices by increasing size.

Rather than showing similar J_{sc} values with increasing device size, **Fig 3.6** shows a decrease in the current density output with larger devices. At this point it was discovered that the number of conductive threads (electrodes) per unit of device area was not kept constant for all devices. This could explain the sharp decrease of almost one order of magnitude in J_{sc} output between the smallest and largest devices. Calculating the number of conductive threads per unit area of device for the smallest (0.194) versus the largest device (0.0129), there appears to be a similar decrease of approximately one order of magnitude. This suggests that device output can be scaled with device size, as long as the electrode density is kept constant.

3.6 Application of Tribo-textiles for Sensing Human Body Movements *in collaboration with Jeremy Gummeson and Ali Kiagadi in the Deepak Ganesan Lab in the Department of Computer Science, University of Massachusetts Amherst*

While much of the recent research in the wireless sensing community has surrounded wearable technology like wristbands, phones, and glasses, one area that has seen relatively little work is smart apparel, i.e. the integration of wearables in clothing. Regardless of this fact, the market for smart garments has grown steadily and is projected to have one of the highest growth rates among wearables in coming years [64]. There is also increasing commercial activity including projects like Google Jacquard, and smart apparel from major clothing manufacturers.

From a sensing perspective, a major advantage of smart clothing is the ability to monitor the signal directly at the location where the signal is strongest. For joint sensing, it allows for measurement at the joint without being limited to locations such as the wrist or waist. The ability to measure individual joints can enable many applications. For example, the knee and ankle joints are important to monitor gait disorders that can occur due to neurological causes like Dementia and Parkinson's, as well as non-neurological causes such as Osteoarthritis, intoxication, and medications (e.g. sedatives). The ability to measure joint movements is also an essential part of balance, posture, and motor control rehabilitation from conditions like stroke, as well as for mass-market athletic performance monitoring.

However, a key drawback of existing textile-based joint sensing technology is that these generally only work with tight-fitting garments, i.e. when the textile is worn as a "second skin". This is for two reasons: a) stretch sensing-based methods [65] use tight-fitting textiles to increase stretch during joint movement, and b) other modalities like inertial measurement units (IMUs), which measure a specific bodily force or angular velocity, and electromyography (EMG), which measures the electrical signals sent to muscles by motor neurons, rely on tight-fitting garments to reduce noise by improving skin contact and reducing motion artifacts. However, a second skin is uncomfortable to wear on a regular basis, and new designs that can be used with loose-fitting, everyday clothing are needed. To achieve this goal requires a radical shift in how we think about smart clothing. Rather than integrate traditional sensors like an IMU or stretch with the textile, we need a clean-slate approach that leverages the unique properties of the textile to enable entirely new ways of sensing using clothing. Specifically, a textile folds, compresses, twists, and scrunches during movement of the joint, and if we can find a way to measure these changes, it can offer an alternate fabric-based way of measuring joints while not requiring tight-fitting clothing.

Toward this end, the following section illustrates the construction and signal detection of a loose-fitting, triboelectric elbow sleeve sensor. The advantage of triboelectric textiles in this instance is two-fold: (1) Because charge transfer between triboelectric textile layers happens due to the relative movement of the layers, it should allow for the measurement of the changes in the textile during joint movement, even when wearing loose-fitting garments, and (2) Because the textile itself is the sensor, it allows the joint to be free of discrete electronics and wires, and placing signal conditioning and other electronics at more convenient locations away from the joint.

A triboelectric textile presents an exciting opportunity, but little is understood of its practicality for sensing when integrated into everyday clothing. Furthermore, a host of noise issues is inevitable, including electromagnetic noise, static potentials, and motion artifacts. These noise issues are exacerbated due to the large surface area and loose fit of the textiles and introduce challenges in how to recover a weak triboelectric signal and sufficiently suppress noise.

Nonetheless the following sections show how these issues were addressed in the de-

sign of a novel fabric-based triboelectric joint sensor, Tribexor, that is simple to manufacture and is able to accurately detect individual joint motions while integrated with loosely worn clothing. The sensor system involves a co-design of the textile and electronics that tackle noise removal and signal enhancement by a combination of textile domain and electronics domain approaches. The final design of Tribexor consists of several discrete, stacked fabric layers that are sewn together and connected to a small form factor, low power amplification circuit and an embedded radio. Attention is also paid to the signal output of the Tribexor sensor, looking at the signal behavior from first principles, and highly discriminating and explainable features are extracted that allow for the detection of joint movement, separate joint extension versus flexion, and estimated joint velocity.

While originally it was intended to leverage such textiles for joint sensing, we stumbled upon an interesting observation during our experiments. We noticed that our sensor can also be used to measure sweating behavior since the triboelectric textile itself undergoes changes due to exposure to sweat. This provides a sensor reading that is equivalent to an Electrodermal Activity (EDA) sensor (alternately referred to as Galvanic Skin Response or GSR. [66]) The ability to monitor joint movements together with sweat levels opens up additional applications such as monitoring hydration while exercising.

3.6.1 Sleeve and Circuit Design

The overall hardware design of Tribexor consists of a smart textile sensor integrated with a small form factor electronic circuit used for amplification and signal conditioning. The sensor consists of a triboelectric-optimized textile patch and is used to collect electrical charge generated by the textile; a multi-stage amplifier circuit is used to amplify the voltage of the tribo signal and reject noise. The central challenge addressed in the hardware design of Tribexor is how to get sufficiently strong signal to noise ratio (SNR) from the textile to detect states of interest. This was addressed both in the design of the elbow sleeve as well as the circuitry, shown in **Figure 3.7**.

The architecture shown in **Fig 3.7** was the result of several design iterations that evolved as the signal output was observed in real-world settings. The first version of Tribexor consisted of a woven arrangement of positive and negative charge carrying threads
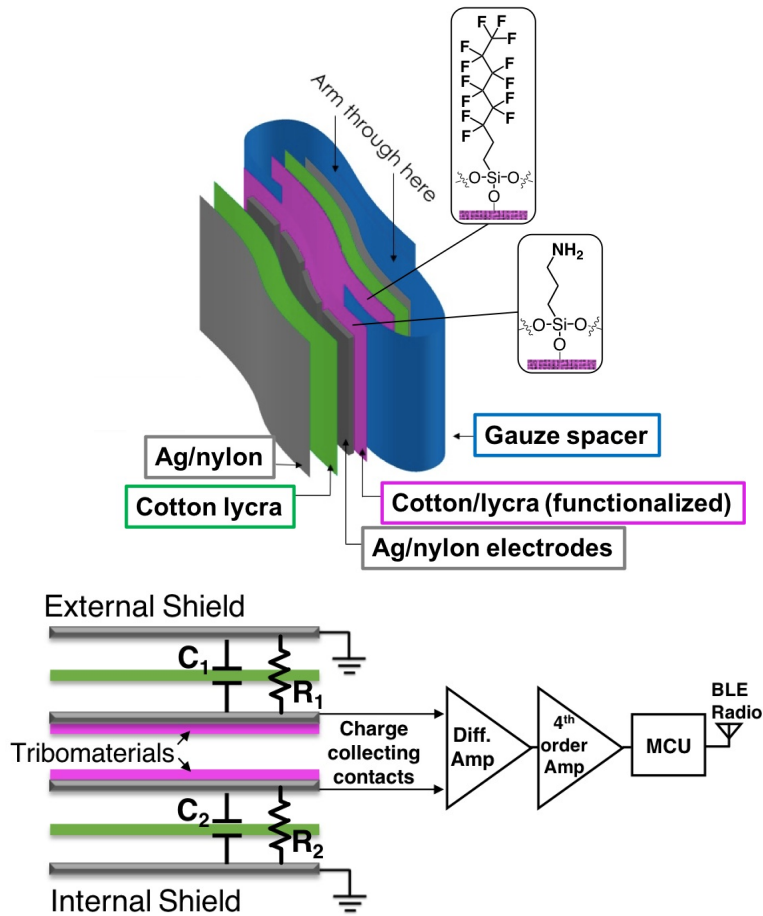
Figure 3.7: Elbow sleeve architecture and circuitry.(Top) Device architecture and (Bottom) Circuit design.

and collection electrodes. We found that the total surface area of interaction between tribo materials was insufficient to produce a significant signal output. The second version of Tribexor saw the transition to the layered design shown. The increased surface area in the layered design allowed us to see significant signal magnitude changes that correlated with joint motion when worn, but we discovered that this DC signal change was actually coupled electromagnetic noise that changed depending on the amount of coupling with the arm that was related to position and not velocity. This observation motivated the inclusion of the differential amplification stage, which caused signal peaks from triboelectric charge and discharge to become visible at the beginning and end portions of individual arm motions. The addition of a microcontroller and Bluetooth low energy (BLE) radio allowed for untethered experiments with mobile users; however, charge/discharge peaks

were observed that correlated with foot impact while walking. This observation resulted in the final prototype that includes signal shielding layers on either side of Tribexor to reduce static field coupling from outside the measured joint.

The final layered textile is comprised of multiple sheets of cotton lycra spandex (90% cotton/10% lycra; Dharma Trading Co.) and silver-plated nylon/elastic fiber (76%/24%; LessEMF) fabrics. The cotton lycra layers were surface functionalized by silane grafting as described previously in this chapter. To assemble Tribexor, the stretchy silver nylon fabric was cut into six 6 in. x 1.5 in. (58.1 cm^2) strips and sewn around the strip perimeters onto the active tribo layers (three strips to a functional layer, making three devices in total.) Another layer of pristine (unfunctionalized, as received) cotton lycra was then attached by sewing around the perimeters of the strips, leaving one short side unsewn for access to electrical wire connections. Finally, a second layer of 8 in. x 8 in. (412.9 cm^2) pristine cotton lycra with a layer of 7 in. x 7 in. (316.1 cm^2) silver nylon stretch fabric centered on the back side was attached around its edges on top of the first pristine cotton lycra layer. Altogether, Tribexor layers from the outside in are as follows: silver nylon, 2 cotton lycras, silver nylon electrode strips, tribo-active layer 1, gauze spacer, tribo-active layer 2, silver nylon electrode strips, 2 cotton lycras, silver nylon. The gauze spacer layer covers one inch inward from the edges on opposite sides of the Tribexor, extending outward on both sides to wrap around the limb of the person testing the device. Velcro strips on the gauze allow the user to adjust the tightness of Tribexor around the limb.

The two outermost shield layers (pristine cotton lycra with silver nylon back) are connected to the differential amplifier with braided wires and adhered to the fabric using conductive adhesive. The two charge collection layers of a single device are connected to the inputs of the differential amplifier with a similar wire and are also adhered using conductive glue.

3.6.2 Addressing a Noisy Signal Response

In its initial stages, the Tribexor included only the active tribo layers sewn to their respective conductive fabric electrodes. However, the signal (voltage output) of the device was masked by noise from different sources. Therefore, both the device architecture and

the circuitry required adjustment before a triboelectric signal could be detected as a result of elbow joint flexion and extension.

While the sources of noise are similar to those observed for other modalities including EMG and electrocardiographs (ECG), there are important differences. The first is form-factor. An electrode has a tiny footprint compared to a textile, which acts as a much larger, noise-absorbing antenna. In addition, when the tribo-textiles are used on loose clothing, the distance between the fabric and skin changes constantly due to body movements, unlike electrodes that are attached to the skin. This results in continuous changes in the coupling capacitance, making it harder to predict and deal with the noise. The second is placement. In the typical ECG, different electrodes are all in contact with the body and therefore absorb a similar magnitude of noise on each. This noise can be filtered by a differential amplifier, which operates by amplifying the difference between two input voltages and suppressing any common input voltages, i.e. noise. However, in the Tribexor, the fabric layers are stacked such that the two electrode layers have different separation distances from the skin, the inner one absorbing noise from the body and the outer one absorbing noise from the environment. This asymmetry means that the noise in the two contacts can be quite different and cannot be completely removed by a differential amplifier.

To reduce the noise and amplify the Tribexor's response signal, multiple steps were taken, including addition of a Faraday cage to the elbow sleeve architecture and adding a differential amplifier and an analog filter to the circuit. The Faraday cage consisted of a layer of plain cotton lycra with conductive silver nylon stretch fabric on the back, as shown in **Fig 3.7** (bottom). These layers were attached on top of each electrode layer to block the noise from the environment and body, respectively. The differential amplifier enhances the output signal of the elbow sleeve in response to contact electrification events. As previously described, it cannot completely reject noise, but it does help greatly attenuate the 60 Hz noise from the building's power lines.

Since there is still significant residual noise after the differential amplifier, additional filtering stages were needed to reduce the noise level. To calculate gain and filtering order of our analog circuit, the goal was to reach a SNR of 10 dB and a final triboelectric signal amplitude of 1V to fully utilize the dynamic range of the analog to digital converter

(ADC) used in the wearable system. The cut-off frequency of the filtering stages was set to be 10 Hz to fully capture the fastest anticipated human movements. The overall gain of the circuit was thus calculated as:

$$Gain_{dB} = 10log(\frac{V_{out}}{V_{in}})^2 \Rightarrow Gain_{dB} = 60dB \tag{3.1}$$

And the order of the filtering stage is calculated in Eqn 3.2.

$$log(\frac{F_{rej}}{F_c}) \times \alpha \times N > 10 - (P_{signal} - P_{noise}) \tag{3.2}$$

Where $\alpha = 20dB/decade$ is the slope of the first order filter, and N is the target order of the designed filter. F_{rej} is the frequency to be rejected (in this case 60 Hz), f_c is the 3 dB cut-off frequency of the signal, and P_{signal} and P_{noise} are the power of the signal and noise, respectively, at the output node of the differential amplifier. Consequently, a fourth-order filtering is required. Taking these parameters into consideration, the circuit was designed as shown in **Fig 3.7** above.

Figure 3.8 breaks down the effect of each stage of adjustment. The initial raw signal is omitted due to its appearance as a flat line where the signal is undetectable. The first stage (results shown in the leftmost panel of **Fig 3.8**) uses only the four-stage amplifier, and the signal corresponding to joint movement can be seen as relatively small peaks in comparison to the noise from walking. Adding a differential amplifier (**Fig 3.8**, bottom, middle panel), the joint movement signal becomes a lot stronger for reasons explained earlier. This stage also removes some of the 60 Hz and static field noise but not all of it. Finally, adding the textile shielding removes most of the noise while retaining most of the triboelectric signal.

3.6.3 Signal Interpretation and Analysis

The first experiments simply show the difference between functionalized and un-functionalized dielectric layers in the Tribexor and the minimal signal difference between
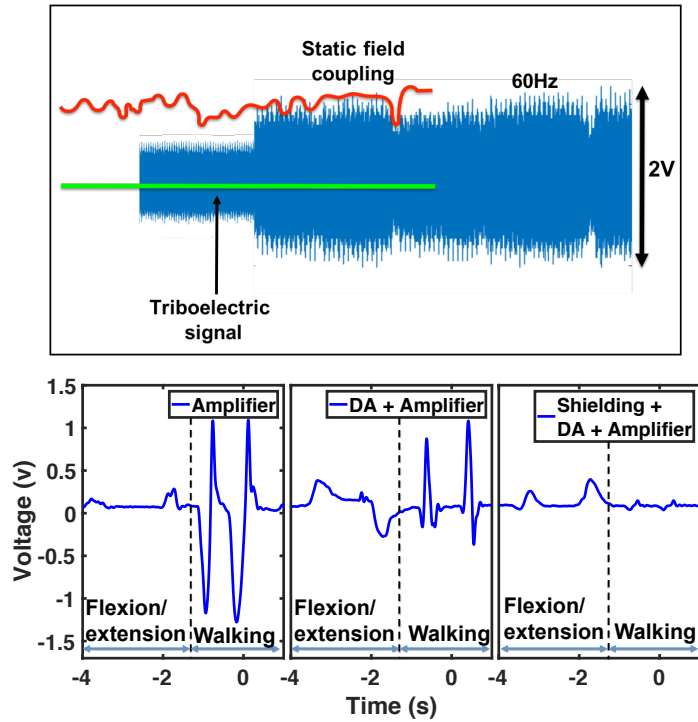
Figure 3.8: Signal before and after filtering. Signal before filters (top) and Tribexor signal response using shielding and amplification (bottom).

wearing it tight- or loose-fitting. Without chemically modifying the cotton lycra surfaces, the output voltage read from the contact/separation of device layers is much lower (**Fig 3.9 (a)**). This is confirmation that the silane grafting was successful. **Fig 3.9 (b)** illustrates the very minor differences in output voltages that result from wearing the device loose- and tight-fitting. The output voltages here are approximately the same, as was the goal for this device.

Let us now turn to analyzing the characteristics of the de-noised signal from Tribexor. Two signals of interest can be observed (**Fig 3.10**). The first is the fast varying changes during flexion and extension of the joint (the phasic component). The second is the slow varying changes due to the state of the joint (the tonic component), which is the change in baseline that can be observed while the joint is stationary. The phasic component is useful for identifying specific joint movements, whereas the tonic component provides information about the wetness and salt content in the textile, thereby allowing it to be used to sense exposure to sweat.
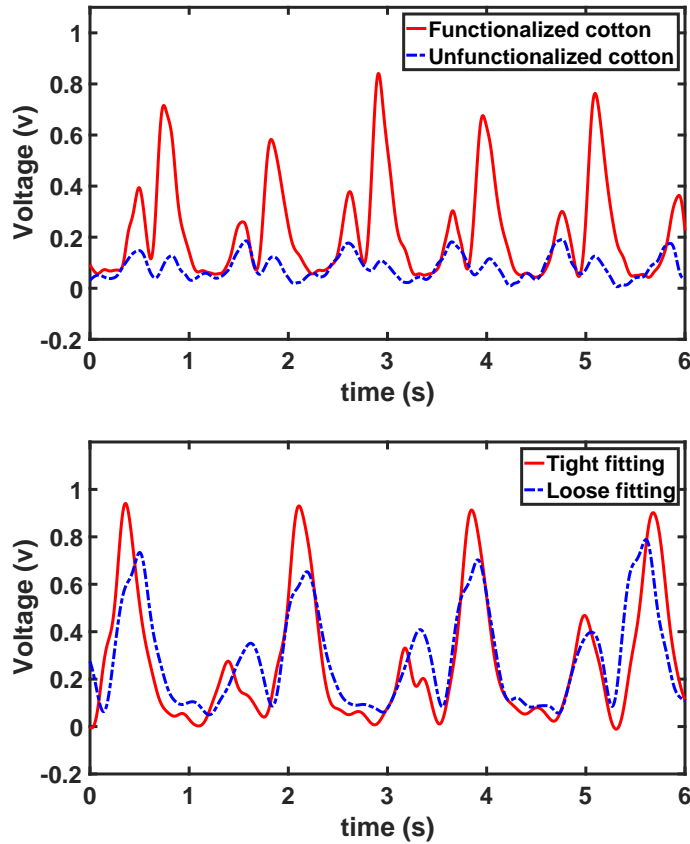
Figure 3.9: Comparison of different signals from Tribexor. **(a)** Functionalized v unfunctionalized cotton lycra layers. **(b)** Tight- v loose-fitting elbow sleeve device.

We first look at the dynamic or phasic component of the time-series voltage signal from the textile sensor and ask how we can map from voltage to the direction of joint movement and the velocity of joint movement. To understand this, we need to obtain an in-depth understanding of the signal characteristics. **Fig 3.10** shows an output instance of an elbow extension (left peak) and flexion (right peak). There are three key parameters of interest: (1) the charge and discharge rates, annotated as θ_1 and θ_2, (2) the baseline voltage when the joint is in the extended vs flexed static position, annotated as β_1 and β_2, and (3) the peak height of the flexion/extension, ϕ. We now explain how these parameters can be used to determine joint state.

The charge and discharge rates (θ_i) of the textile vary according to the start and end state of the textile. At the start of an extension motion, the textile is in a compressed state. As the arm is extended, the layers separate, causing a voltage peak at roughly the
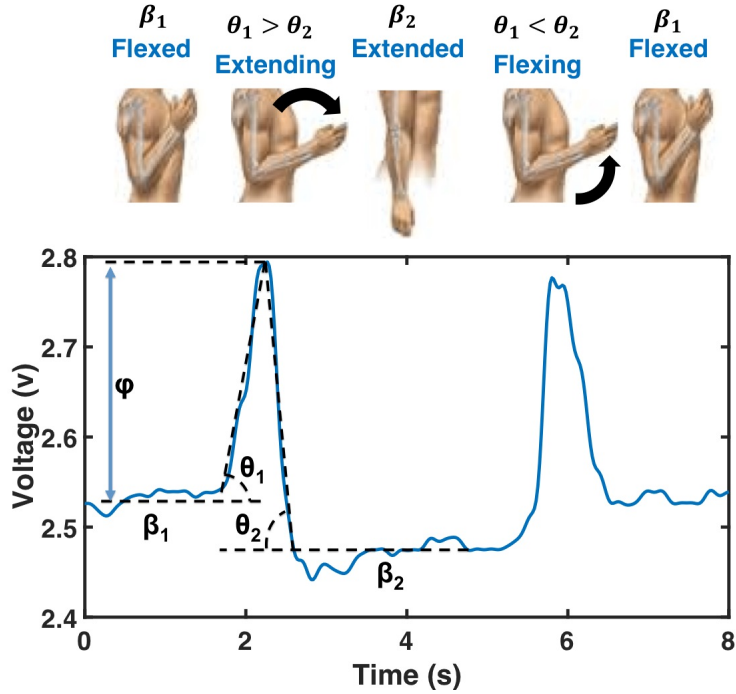
Figure 3.10: Signal characteristics of elbow joint flexion and extension.

midpoint of motion; the voltage subsequently decays because of conductive paths between the textile layers. During a flexion action, the same signal features occur, but at different relative rates. Initially, there is much less surface contact between the textile layers; during motion a peak still occurs because of separation but at a slower rate. The final state of the textile is a compressed state which results in fast voltage discharge because of more conductive paths available between the textile layers. As a result of this behavior, we consistently find that $\theta_1 > \theta_2$ during extension, and $\theta_1 < \theta_2$ during flexion, as indicated in **Fig 3.10**.

The signal baseline (β_i) also changes depending on whether the joint is in the flexed vs extended static position. There are two reasons behind the change. First, the effective surface area and intimacy of contact with the skin will vary as a joint opens or closes. We expect that more EM noise is injected when capacitive coupling is higher, while less is injected when coupling is lower. Second, the impedance between the electrodes and ground plane shielding cause asymmetric signal changes at the input of the differential amplifier. The inputs of the amplifier are the base nodes of bipolar junction transistors. As the impedance of electrodes changes, the bias current of the differential amplifier changes,

which results in a very small voltage shift in the output of the differential amplifier. This offset, though small, is amplified and is observed as a baseline shift i.e. $\beta_1 > \beta_2$ (**Fig 3.10**).

The peak height (ϕ) depends on the velocity of the joint since the tribo layers move more quickly relative to each other, relating in more compression and expansion and therefore greater amount of charge transfer.

From a detection standpoint, these observations give us explainable features that can be used to distinguish between joint states. Such explainability is increasingly important, particularly when designing robust classification methods.

3.6.4 Determining Arm Flexion and Extension

Our first set of benchmarks looks at how well we can separate flexion versus extension of the elbow using the features shown in **Fig 3.10**. We only look at the utility of the two core features θ_i and β_i to understand how useful these two features are to performance.

Motion data was collected by having a user perform flexion and extension arm motions for 5 minutes. The resulting data was then used to train a logistic regression-based classifier dependent on those two features. The classifier was then tested on the same user for data during different experimental conditions. To demonstrate the robustness of classification to moisture, noise induced from walking, and changes in textile position on the user's arm, we tested the classifier for the user in those conditions.

Results for this binary classification are summarized in **Table 3.2**; the motion classifier program was able to detect flexion and extension with the elbow sleeve with very high precision and recall across a range of conditions. The best results were measured during benchmark experiments when moisture was introduced – it was observed that Tribexor achieves perfect precision and recall as a consequence of larger shifts in DC baseline magnitude. The worst results were obtained from benchmarks collected while a user was walking, but still yielded precision and recall values of 88.1%; we hypothesize that small shifts in the textile location on the arm and low amplitude static coupled noise could result in low-velocity arm motions being mis-classified.

Table 3.2: Binary classification of signal detection

	Flexion		Extension	
	Precision	Recall	Precision	Recall
Same position	.994	1.00	1.00	.994
Different positions	.964	.986	.989	.968
Moisture	1.00	1.00	1.00	1.00
Walking	.881	.881	.881	.881

3.6.5 Determining Velocity of Arm Movements

The minimum sensitivity of Tribexor is explored in this section, i.e. the minimum speed at which the joint must move for the Tribexor to be able to capture the signal. The typical peak angular speed for an elbow joint during curl exercises is 200 deg/sec [67]. Therefore, the objective is to be able to detect a signal well below this peak speed so that the entire flexion and extension motion can be captured.

Given this requirement, the angular speed can be converted to a minimum SNR required for the triboelectric signal. Because the main source of noise is the 60 Hz signal from power lines, we need to first characterize the noise level and then look at what the triboelectric signal should be in order to detect it above the noise. The 60 Hz signal was characterized across different environments including three buildings and one residential house, finding that Tribexor typically outputs the 60 Hz signal with an amplitude of 100 mV. This means that in order to achieve a minimum SNR of 0 dB during elbow flexion and extension, the minimum triboelectric signal amplitude must be at least 100 mV.

For example, to detect movement with 100 deg/sec velocity, we would need to be able to detect a minimum signal of 1 mV/(deg/sec) as shown below:

$$S_{min} = \frac{V_{peak}}{\omega_{peak}} = \frac{100mV}{100deg/sec} = \frac{mV}{deg/sec} \quad (3.3)$$

Figure 3.11 shows how well Tribexor can capture joint movements when a user is flexing and extending their arm at moderate speeds. We see that the minimum sensitivity is roughly 50 deg/sec, so we can easily capture normal joint movements. The reason for this minimum threshold is that slow joint movements produce a triboelectric signal that is too weak to be detected. This can be addressed by using automatic gain control (AGC) to adjust gain; however, our current design uses a fixed gain. Once we cross the minimum sensitivity, Tribexor tracks the ground truth signal very accurately. These benchmarks show that Tribexor is a reliable joint sensor and is sufficiently sensitive to capture normal hand movements.
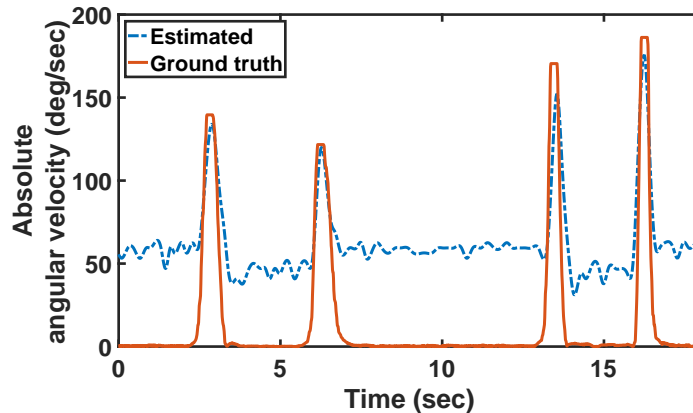
Figure 3.11: Detection of flexion/extension at moderate speeds.

Next, we look at how well Tribexor can estimate angular velocity across multiple wears of a textile. While in general the voltage extracted is highly correlated with the angular speed, loosely worn textiles like sweatshirts are often worn over different inner layers. In addition, the fabric folding and compression may differ slightly each time the textile is worn leading to signal differences.

To characterize the error, we asked the user to remove and re-wear the shirt five times. We then used five-fold cross validation where we calibrated the sensor from data from four of the times the textile was worn, tested the performance on the held-out data, and repeated five times. **Figure 3.12** shows a cumulative distribution of the error, i.e. the probability that the percent error in angular velocity detection is less than or equal to the

x values on the graph. Our results show that, as expected, there is error due to differences across the times when the textile is worn. But we also see that the median angular velocity error is only 11%. In other words, there is a 50/50 probability that the percent error is less than or equal to 11%. This means that despite the fact that Tribexor is integrated with loose clothing, it provides a reasonable estimate of the velocity under natural settings.
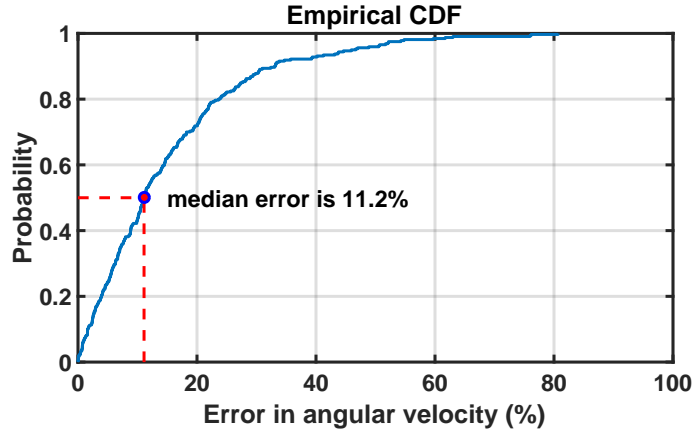
Figure 3.12: Cumulative distribution of error in angular velocity. Estimation across multiple wears of the textile.

3.6.6   Determining Sweat Level

So far, we have looked at the dynamic or phasic components of the triboelectric signal. We now turn to the slowly varying baseline signal or the tonic component. While sweat monitoring was not the original intent for use of the elbow sleeve, initial experiments revealed that the baseline signal varied due to sweat, which can be used as an additional sensor signal.

The reason sweat affects the tribo signal is because the wetting happens in one direction — the inner layers absorb more sweat, whereas the outer layers that are close to air are dryer. This results in an impedance difference between the outer and inner electrodes. As depicted in the circuit diagram (**Fig 3.7**, top) R_1 and R_2 represent the impedances between the outer electrode and shielding layer and inner electrode and shielding layer, respectively. Since sweating initially affects internal layers, it reduces R_2. As a result, a small DC offset is generated at the output node of the differential amplifier. This small

voltage is then amplified in the electronics circuits to create an observable change at the output of Tribexor.

The sweat-induced changes can either be viewed as a useful signal to measure sweating behavior or as noise that confounds the joint measurement signal. If viewed as noise, the insulation layer between the shielding layer and charge collecting electrodes can be covered with a hydrophobic coating for protection from water [68]. In this work, we look at sweat as a useful biochemical signal that can be captured by Tribexor in addition to its use as a joint movement sensor.

To understand the device's sweat sensing capability, we empirically explored the correlation between the voltage output obtained from Tribexor with a variety of other measures — salt concentration, water volume, and skin conductance from a galvanic skin response (GSR) sensor. The results shown are based on a rather laborious process of wetting the sensor in a particular way and blow drying before using it again. To begin, Tribexor was analyzed for how well it can detect the concentration of sweat. A controlled measurement setup was designed wherein the textile was sprayed with salt water of 40 mM NaCl concentration, which is similar to that of human sweat. [42] The textile was wrapped around a cylinder-shaped object that acted as a human elbow. During the measurement, the textile was placed on top of a precise digital balance to manually record the amount of salt water added to the textile. To better simulate human sweat, the rate of water deposition was adjusted to match the normal rate of human sweating. According to the literature [69], the average human sweats at rate of 13 mL/min. The arm accounts for roughly 10% of the body's surface area [70], so it was assumed that roughly 1.3 mL/min is generated by the joint. Salt water was applied on the front half of the textile, which covers around 1/6 of a human arm. Therefore, solution was sprayed on the textile at rate of 0.2 mL/min to best mimic human sweating. During this experiment, the only significant information comes from the changes in the baseline signal, i.e. β in **Figure 3.10**, we use a low-pass filter to remove triboelectric signals generated from hand movements. The result is that only the baseline changes due to salt-water accumulation.

Figure 3.13 shows the changes in baseline, β, as a function of salt water volume. The voltage baseline has a clear second order polynomial relation to salt water volume

with a low root-mean-square error of 0.1 V. While there will be natural variations in sweat accumulations in the textile due to evaporation, our results are promising since it provides a fabric-based method to measure sweat.
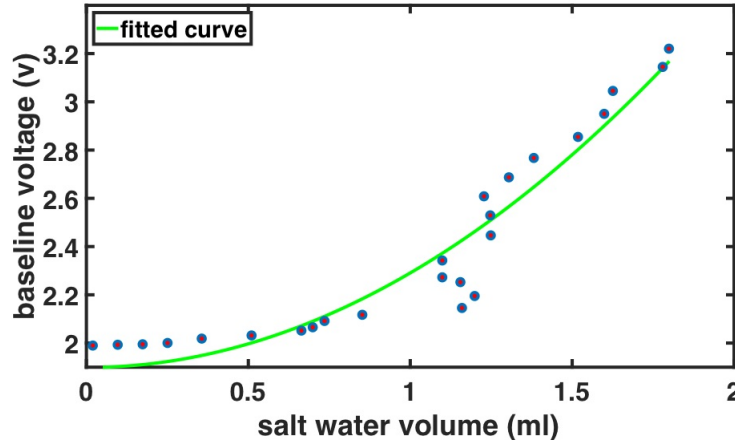
Figure 3.13: Tracking saltwater level with baseline voltage.

Another capability of Tribexor is detection of the sweat concentration on a user's skin during strenuous activities. This provides an additional metric of exertion for the user on top of running speed or heart rate. For this experiment, a user wore the Tribexor on one elbow while wearing an Affectiva Q sensor on the wrist. [71] The Q sensor provides an indirect measure of skin moisture level by using skin conductivity as a proxy. Here it works as a standard with which to evaluate the effectiveness of Tribexor. To detect sweating and reject high-frequency noise, a low pass filter was applied to the signal output. The resulting output represents a baseline for different elbow states.

The user was asked to perform a combination of walking and running on a tread-mill. There were no restrictions on running or walking speed, arm position or swing, or rest periods where the user consumed water. Tribexor's output was collected at a sampling rate of 50 Hz, while the Q sensor was configured to use its maximum sampling rate of 8 Hz. The two sensor streams used a common clock to synchronize prior to the start of the experiment. **Figure 3.14** below shows the extracted signal baseline together with the skin conductivity measurement. The results show that the signal provided by Tribexor closely tracks the signal from a GSR sensor and simultaneously provides more information about the user's activity state.
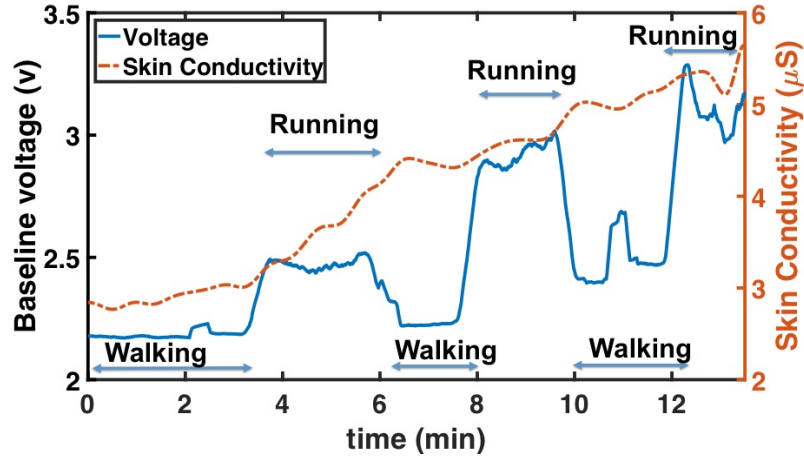
Figure 3.14: GSR skin conductivity vs. Tribexor moisture level.

If we consider the way these two devices function, their signal similarities should be expected. A GSR sensor monitors skin conductivity between two electrodes placed on the skin. Therefore, as the user sweats more, the skin becomes more conductive, and current flow increases between the electrodes. Similarly, the Tribexor signal increases with sweat accumulation, as the sweat reduces the electrical resistance across the textile. Hence the Tribexor signal closely tracks the GSR signal, gradually increasing as the user continues to sweat. This experiment thus demonstrates a novel textile-based version of a galvanic skin response signal that requires no electrodes.

In addition to the overall increase in baseline voltage in **Fig 3.14**, it should be noted that the phasic (dynamic) component of the signal also shifts when the user is walking vs running. This is because the elbow state is different in walking and running. Users run with their elbows bent, and doing so increases the compression between the grounded shielding layers and charge collection layers. This results in a shift in the baseline resulting in a higher voltage level. When the user starts walking, the elbow is much more extended and results in a reduced baseline. Thus, we see that by analyzing the phasic and tonic components of the signal we can obtain complementary information about the joint.

3.7   Summary

Chapter 3 showed that silane grafting is an effective method to modify fabric surfaces towards the enhancement of triboelectric properties of the textiles. Using this method, different triboelectric devices were constructed, demonstrating the utility and practicality of solution functionalization for bulk cotton-based fabric electronics. The thickness and scalability of the devices were probed for a more basic understanding of the effects of device architecture on triboelectric output. Results showed that thinner cotton fabrics yield higher currents, and the devices are scalable when electrode density (number of electrodes per unit area) remains constant. These concepts were used to guide the construction of a triboelectric body-motion-sensing sleeve. Unlike other sensing clothing, the sleeve presented in this work could be worn loosely on the body. The tribo sleeve was able to accurately detect angular velocity movement of an elbow above 50 degrees per second, and using the sleeve, data could be differentiated to accurately determine flexion and extension events across multiple conditions, including when the sleeve was in different positions on the arm, when the user was walking, and when the sleeve was wetted with water. This type of loose-fitting garment is extremely promising for applications in tracking rehabilitation in patients with skeleto-muscular injuries or body movement limitations as a result of other conditions, like stroke or traumatic brain injury. Future work that could improve performance and viability of device commercialization may include incorporation of the signal processor into the textile design and adjustments so that the triboelectric output can be harvested to minimize or eliminate the need for power outside of the sleeve.

CHAPTER 4

iCVD: A DRY METHOD FOR
FUNCTIONALIZING TEXTILE SURFACES

4.1 Introduction

In Chapter 3 we saw that silane grafting in solution could be used as a facile means to modify cotton-based fabric surfaces toward triboelectric textile devices. However, solution processing of textiles is widely known to pollute water resources, [72] and silane grafting limits the textile substrate to natural fibers like cotton that have hydroxyl groups on the surface due to their cellulosic composition. With these drawbacks in mind, a new method for modifying textile surfaces was investigated. Denoted iCVD for initiated chemical vapor deposition, this method not only broadens the variety of materials that can be used to functionalize textiles, but it also nearly eliminates solution waste and the pollution that accompanies it. Furthermore, iCVD is known for its conformal coating of substrates, [73] which is especially significant when coating rough surfaces such as textiles.

Chapter 4 therefore describes in detail the construction from scratch of a vacuum chamber made specifically for iCVD coating of textile substrates. Using this "dry" method for modifying textiles, the resulting dielectric surfaces were compared to those described in Chapter 3 that were made by silane grafting in solution. These two types of coatings were investigated and compared in terms of both coating adhesion strength as well as triboelectric output in order to understand the effectiveness of each method.

4.2 Initiated chemical vapor deposition for textile surface functionalization

Initiated CVD is a recently-developed technique for depositing thin films of polymers onto various substrates. [74, 75] Because the polymers are formed on the substrate

surface in the vapor phase, this method enables conformal coatings on patterned, rough, and even liquid-phase substrate surfaces and is thus ideal for chemically modifying the rough surfaces of textiles. [56, 76–79] Other advantages to iCVD over alternative thin film deposition methods include that it is a low-energy process, pendant groups and the substrate surface are left intact, no solvents are required, and it allows control over copolymerization, deposition rates, and even film thicknesses down to 10 nm. [80]

The iCVD method is ideal for functionalizing soft and rough materials because no damage is caused to the substrate surface, and the resulting thin films completely and conformally coat all exposed surfaces, rough or smooth, patterned or unpatterned. [73, 81] In terms of textiles, iCVD has been previously used to conformally coat electrospun mats with fiber diameters on the order of 600 - 2200 nm. [82] In addition to maintaining surface roughness, the monomer pendant groups are left fully intact in the resulting polymers, [82,83] which is not always the case with plasma-enhanced CVD and sputtering techniques, for example.

In addition to advantages over dry processing methods, iCVD has a distinct advantage over solution-phase processing because it requires no solvents. Solventless thin film deposition is especially useful both for depositing on water-sensitive surfaces like paper and also for eliminating any waste involved in other processes typically used to functionalize surfaces such as solution grafting, dyeing, dip-coating, or spin-coating. On top of producing massive amounts of solvent waste, dyeing, dip-coating, and spin-coating also tend to result in non-uniform functionalization across textile surfaces due to random agglomeration of functionalizing material, which compromises adhesion capability as well. [84] Another advantage of iCVD is deposition control, not only in terms of film deposition rates and thicknesses but also in the variety of polymers and copolymers that can be achieved. Initiated CVD is known for its high rates of deposition (100s of nm per minute) and film thicknesses controllable down to approximately 10 nm. [85–87] There is also an enormous variety of polymers and copolymers achieved with iCVD to date with an equally large variety of applications, including electronic devices, thermal sensors, hydrophobic and hydrophilic coatings, microfluidics, and anti-fouling surfaces. [85–87]

With these advantages in mind, a custom iCVD chamber was constructed in order

to conformally coat textiles with insulating (dielectric) polymers. As depicted in **Figure 4.1**, the chamber consists of a shallow, stainless steel well (25.4 cm diameter, purchased from Kurt J. Lesker) with multiple ports for electrical and chemical feed-throughs, pressure control, and vacuum pump attachment. Vacuum flow (Edwards RV8 vacuum pump) is directed across the chamber by placing the vacuum pump outlet opposite the chemical inlet ports. Effluent chemicals are condensed in a stainless steel liquid-nitrogen trap (Kurt J. Lesker) that sits upstream from the vacuum pump to prevent pump oil contamination.

The heated filament array was constructed in-house using Nichrome-80 wires (Omega Engineering, 24 AWG) wound around ceramic-encased screws tapped into a thin copper block, which in turn is affixed to a power feed-through by a screw. When fixed in the chamber, the filament array wires cover approximately 103.2 cm^2 of stage area and sit approximately 2.54 cm above it. Filament temperatures are set using the Variac power supply and monitored by an insulated thermocouple wire affixed to the chamber wall that is suspended in the space directly between the filament wires.

The stage (chamber floor) is back-cooled (Neslab RTE-7 recirculating chiller) for control of substrate temperature, which is monitored by a thermocouple affixed to a silicon wafer placed underneath the filament array during deposition.

Monomers are flowed into the chamber from either glass (blown in-house) or stainless steel (Swagelok) vials. The vials and feed-in lines are heated by wrapping with heating tape (Omega Engineering), which is insulated by wrapping with aluminum foil in order to maintain temperature stability and uniformity throughout the line. Monomer and initiator heating tape temperatures are controlled using J-Kem temperature controllers.

Pressure in the chamber is monitored with both a Baratron capacitance manometer (MKS Instruments, model 626) for pressures below 1 Torr and a Stinger gage (InstruTech) for pressures from 1 Torr to ambient. The Baratron gage is electrically connected to an MKS throttle valve (model 253B) and pressure controller (model 651C), which together provide control over both the deposition and base pressures.

The iCVD process is meant to polymerize monomers specifically prone to radical-initiated polymerization, such as acrylates. [88] **Figure 4.2** shows the reaction chemistry
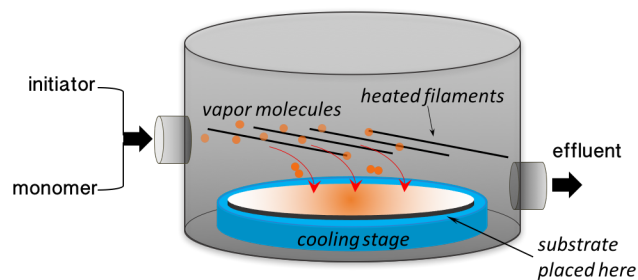
Figure 4.1: Illustration of the iCVD chamber.

for a fluorinated acrylate monomer *1H, 1H, 2H, 2H*-perfluorodecyl acrylate (PFDA). This scheme is relevant to all acrylate monomers discussed in this work.
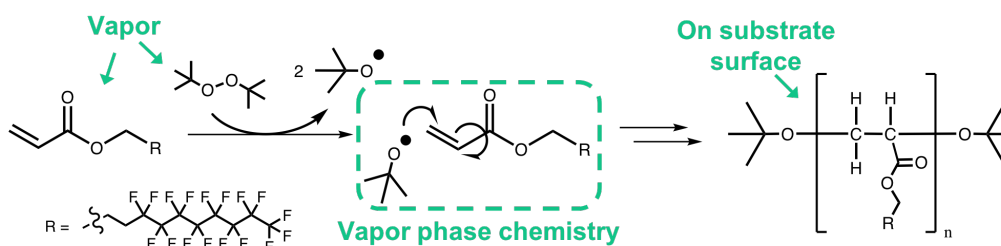
Figure 4.2: iCVD polymerization of acrylate monomers. Shown here with PFDA.

During deposition, the nichrome filament array is heated electrically with a Variac AC power supply to approximately 300°C to initiate radical formation of di-tert-butyl peroxide (TBPO), which is used as the initiator for all iCVD reactions in this chamber. At the same time, the monomer vapor is flowed in and attacked by the initiator radicals after adsorbing to the back-cooled substrate surface. The resulting polymer film thickness is dependent on many variables including monomer vapor pressure and flow rate, initiator vapor pressure and flow rate, base pressure in the chamber, deposition pressure, and stage and filament temperatures. [83, 88] For this chamber, monomer and initiator flow rates are controlled manually by a needle valve on each port (purchased from Swagelok). Although a quartz crystal microbalance can be added to the chamber to measure deposition rate, this chamber is not equipped with one; therefore, polymer film growth rates and thickness cannot be measured in situ, but thickness can be measured post-deposition with profilometry using a silicon wafer substrate.
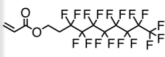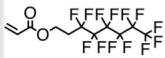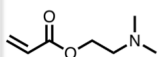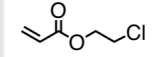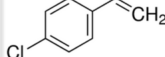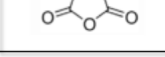
Studies have shown that the reaction kinetics of polymer formation during iCVD are most significantly influenced by monomer fractional saturation (partial pressure /saturation pressure or P_M/P_{sat}) and the temperature of the cooled stage. [86, 87] This makes sense if the monomer must be present for polymerization to occur, and for the monomer to be present on the substrate, the substrate must be cool enough for condensation. A more in-depth study was executed that supports this claim, wherein polymers were iCVD-ed onto a surface patterned with trenches of different aspect ratios. [89] This study correlated two very significant concepts: (1) P_M/P_{sat} dictates the concentration of monomer adsorbed on the substrate surface and the initiator's sticking probability and (2) Sticking probability is highly dependent on monomer fractional saturation due to the comparatively larger time scale of acrylate polymer propagation under iCVD conditions (230 μs) [90] than initiator desorption from the substrate surface (33 μs). In other words, higher monomer fractional saturation yields higher initiator sticking probability because initiator cannot chemisorb to the surface (initiate polymer propagation) without monomer present. Conformality of polymer to substrate is a direct result of polymerization occuring on the substrate surface. [81, 91]

4.3   Reaction Conditions for Different Monomers

Because the chamber was made in-house, polymer deposition control is somewhat limited, and film thickness can vary from one deposition to the next. Nonetheless, a number of acrylates were successfully polymerized, and their deposition parameters, structures, and resulting thin films were recorded for future chamber users in **Table 4.1**. The polymer film thickness column indicates the date of the polymerization from which the data was taken, except for the PFDA reaction, which was successful with similar deposition conditions on multiple dates.

There were also a number of deposition attempts to polymerize other monomers that were unsuccessful for various reasons. These depositions are listed in **Table 5.1**, along with further explanation.

Table 4.1: iCVD conditions of successful polymerizations.

Monomer Structure	Name	Properties (MW; P_{vap}; T_{bp})	P_{base} (Torr)	P_{dep} (Torr)	$P_{setpoint}$ (Torr)	T_{mon} (°C)	Needle valve turns (mon.; init.)	Dep. Time (mins)	Polymer Film Thickness (μm)
	PFDA	518.17 g/mol --- 90°C (4 Torr)	< .300	.400	.400	85	1;1/4	20	5-7
	3,3,4,4,5,5,6,6,7,7,8,8,8-Tridecafluorooctyl acrylate	418.15 g/mol --- 76-80°C (8 Torr)	<.300	.400	.400	80	1;3/8	10	Indeterminable; too sticky (04-05-18)
	2-(Dimethylamino)ethyl acrylate	143.18 g/mol 18.1 Torr(20°C) 64°C (12 Torr)	<.300	.613-.350	---	50	1.5;3/8	10	.12 (03-16-18 #3)
	2-chloroethyl acrylate	134.56 g/mol --- 124-127°C (760 Torr)	<.300	1	1	50	½;1/4	15	1.1 (4-27-18)
	4-chlorostyrene	138.59 g/mol 0.68 Torr(20°C) 192°C	.300	.250	---	75	1;1/4	30	.170 (02-20-18)
	Maleic anhydride (co-chlorostyrene)	98.06 g/mol 0.16 Torr(20°C) 202°C	.185	.334	---	100	2(Cl-styr);1/2(M.A.); 1/4	10	11-17 (03-12-18)

4.4 Comparison of Wet and Dry Coating Methods

To compare the wet and dry methods for surface functionalization, silane-grafted (Si-F) and iCVD-ed (PFDA) regular cotton swatches were analyzed via XPS, SEM, contact electrification with nylon, and changes in water droplet contact angle with the surface before and after 10 minutes of rubbing against regular cotton. It should be noted that the acrylate used in the iCVD method (PFDA) contains 4 more fluorines (i.e. 17 versus 13) in its fluorocarbon chain than does the perfluorooctylsilane (Si-F) moiety, and one might argue that this creates an inequivalent comparison between the functionalization methods. However, a silane species with 17 fluorines was not commercially available, and the acrylate species with 13 fluorines yielded very sticky, adhesive-like thin films unlike the PFDA films. Nonetheless, the species are comparable in that both yield a reasonably long fluorocarbon chain on the surface of the substrate.

To confirm the presence of fluorine on the cotton surface after each functionalizing method was employed, XPS was performed. The results in Figure 4.2 show a peak for the

F1s electrons (680 eV) in the silane-grafted (Si-F) and iCVD-ed (PFDA) cotton samples, but no similar peak for pristine cotton (**Fig 4.3** middle), as expected. Also significant is the fact that for the pristine cotton sample, the C1s peak is very prominent, whereas for the fluorinated cotton samples (top and bottom), the C1s peak is minimized, but the F1s peak dominates. Finally, it should be noted that the fluorinated cotton samples show splitting of the C1s peak into two peaks, one representing non-fluorinated carbons, and the other the fluorinated ones.
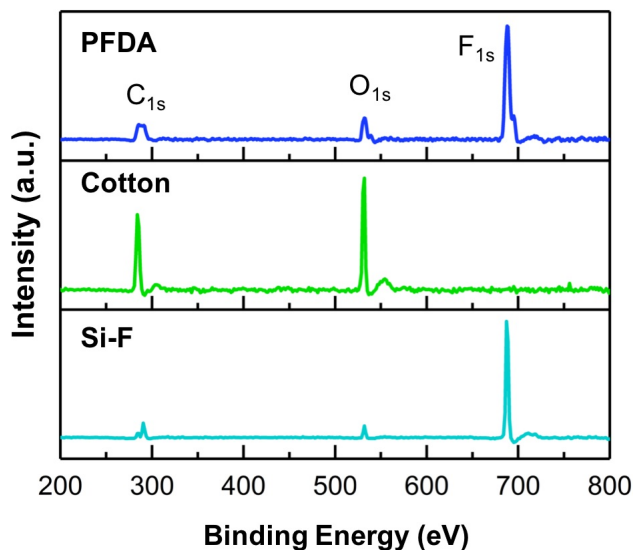
Figure 4.3: XPS data of functionalized and unfunctionalized cotton fabric.

The functionalizing methods were tested for adhesion to the cotton fabric by rubbing against cotton for ten minutes. SEM images in **Figure 4.4** below give some insight into the durability of each coating method, showing silane-grafted (left) and iCVD-ed (right) thread surfaces before (top) and after (bottom) rubbing. The two images on top show a single thread pulled from each of the respectively-coated cotton fabric swatches after functionalization. Both methods appear to yield conformal and even films around the thread filaments. However, after rubbing there appears to be a difference between the silane-grafted (Si-F) and iCVD-ed (PFDA) samples, wherein the silane-grafted film is much more damaged than the iCVD-ed film. Still, the images are somewhat affected by charging that occurs due to the SEM electron beam electrifying the very dielectric surface. A 3 nm gold film was sputtered on the samples prior to imaging, but some charging is still visible, due

to the extreme dielectric nature of the fluorinated surfaces.
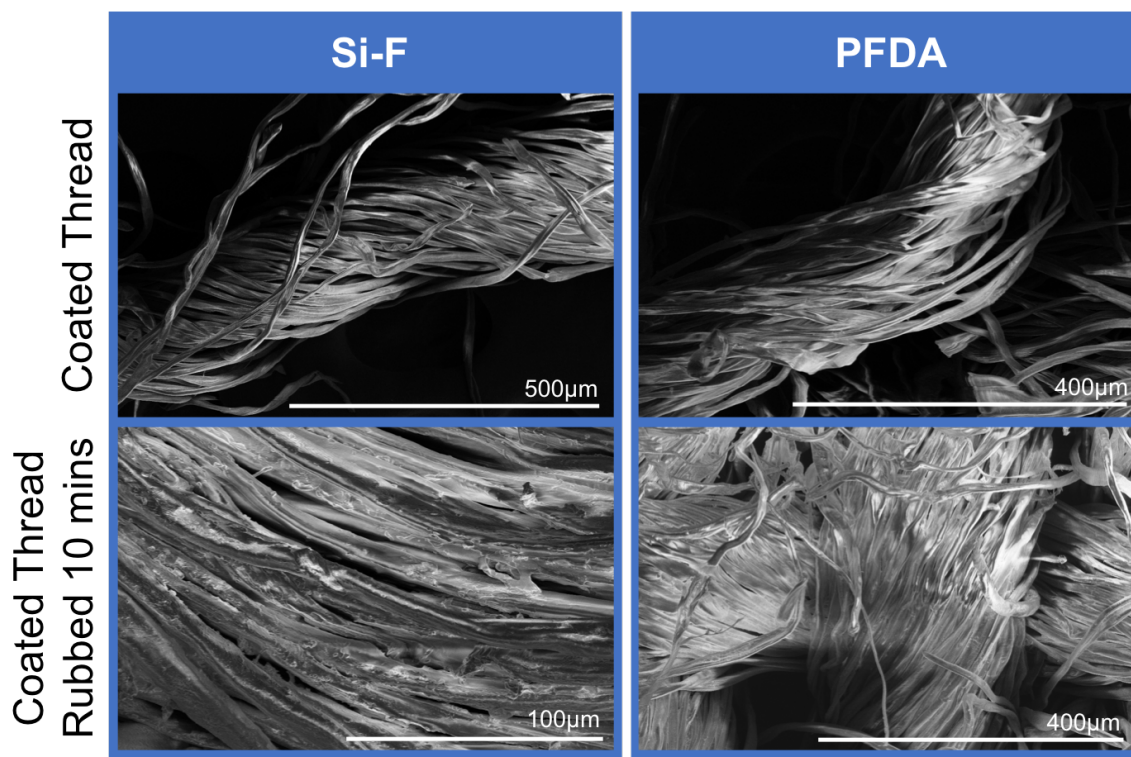
Figure 4.4: SEM images of cotton abrasion tests. Functionalized cotton before (top) and after (bottom) rubbing with cotton fabric for ten minutes.

To confirm the effects of rubbing (abrading) the functionalized samples, they were further compared by testing contact electrification using the triboelectric vertical contact mode setup described in Chapter 1, along with comparing water droplet contact angle with the surfaces. The results of the short-circuit current tests and contact angle changes are shown in **Figure 4.5**. To give an idea of the observed tribo signals, the graph in **Fig 4.5(a)** plots current output versus time for a similar number of contact/release events for each device. By looking at the graphs of the signals, it is obvious that the signal magnitudes are very similar regardless of the method of functionalization. However, the signal response to contact/separation events can vary from one event to the next. Therefore, to confirm similarity in the overall outputs of the devices, data was collected for three trials of twenty seconds each and statistical evaluation was performed using absolute values of the peak heights from each trial, as displayed in **Fig 4.5(b)**. Looking at the statistics, the average peak heights for solution- and iCVD-functionalized fabrics are very close, but the maximum

values and therein the ranges for the respective functionalizing methods are very different, with those for iCVD being almost twice as high. Still, the signals are on the same order of magnitude.
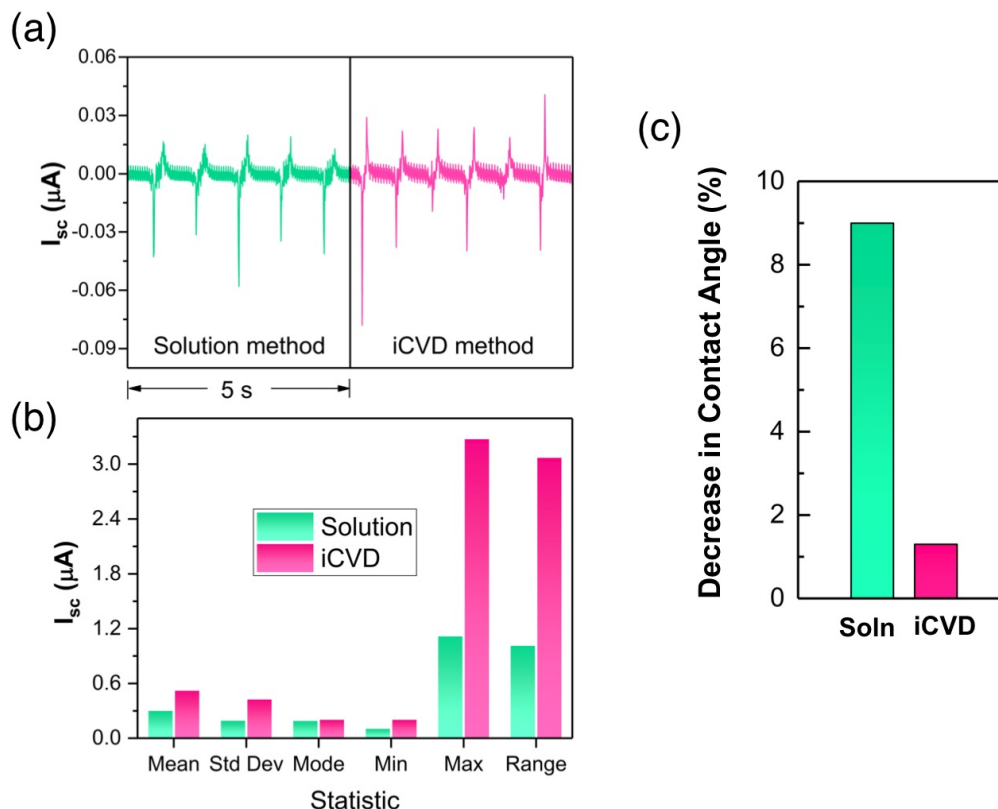
Figure 4.5: Wet vs. dry chemistry methods. Comparison of Short-Circuit Current via **(a)** Signal Response **(b)** Statistics Using Peak Heights from Multiple Signal Response Trials, and **(c)** Decrease in contact angle after 10 minutes of rubbing against cotton.

The most significant difference in the two methods can be observed with the water contact angle change after rubbing for ten minutes with cotton fabric (**Fig 4.5(c)**). Fluorinated surfaces are known for their hydrophobicity, and a greater contact angle between the water droplet and surface therefore indicates greater hydrophobic character. Thus, abrasion of the fluoropolymer can be inferred from a decrease in water droplet contact angle with the surface. The data in **Figure 4.5(c)** confirms the SEM observation that the silane-grafted fluoropolymer is less mechanically stable and wears away more easily than the iCVD-ed fluoropolymer (9% decrease vs 1% decrease, respectively). These results were obtained from just ten minutes of rubbing with cotton, and this emphasizes the instability of the silane-grafted films.

4.5   Summary

Chapter 4 illustrates a dry method (iCVD) for functionalizing textile surfaces. This method has been studied in depth and is known to have many advantages over other thin film deposition methods in that it is a low-energy process, results in conformal films, requires no solvents, and allows a high degree of control over film deposition rate and thickness. Chapter 4 also describes an iCVD chamber that was constructed from scratch to deposit conformal polymer coatings on textiles. Fluoropolymer films were deposited on cotton substrates and compared to those from Chapter 3 that were silane-grafted onto similar cotton fabric. Although initially the films are optically similar, their adhesion properties are quite different and much better for the iCVD-ed fluoropolymer films, as evidenced by the decrease in water droplet contact angle and SEM images after rubbing with cotton for ten minutes. The silane-grafted fluoropolymer films showed very weak adhesion via decrease in water contact angle of 9% compared to 1% for iCVD-ed films. Therefore, although their electrical performances are similar, the films are not equally stable over time, and the iCVD-ed film ultimately outlasts its solution-processed counterpart.

CHAPTER 5

USING VAPOR CHEMISTRY TO ACHIEVE IONICALLY CONDUCTIVE TEXTILES

5.1 Introduction

As with any portable electronic device, a viable smart garment requires a means to store some amount of useable power. This poses a great challenge for smart textiles where form factor imposes strict parameters such as the extreme flexibility and breathability of typical clothing in addition to being washable. To date no flexible battery, supercapacitor, or even textile supercapacitor meets these criteria completely. For portable devices, the ideal storage component would be a supercapacitor because they exhibit characteristics such as high power density, short charging time, and long cycle life. [92] Considering these properties, textiles could serve as a viable platform on which to base a supercapacitor, given their multiscale roughness that maximizes surface area, which could in turn maximize power density. However, one issue with putting any supercapacitor in a garment is the electrolyte, as conventional electrolyte materials tend to be chemically unstable or acidic liquids and gels. [93] For example, proton conducting gels function using sulfuric [94] or phosphoric [95] acids, which could corrode a textile over time. In addition, liquid electrolytes pose the potential problem of leaking out of the encapsulation material more so than do gels, although neither is optimal for a textile platform.

To circumvent the issues involved with conventional electrolytes, new electrolyte materials have been sought, the most prominent of which for this work are poly(ionic) liquids (POILs). Consisting of an ionic polymer species stabilized by a counterion, POILs have recently been investigated as solid state electrolytes due to their high conductivities ($10^{-4} S/cm$ at 25°C), chemical and thermal stability, flexibility, durability, and low volatilities. [96, 97] The fact that these electrolytes are polymeric suggests that iCVD could be invoked to deposit conformal POIL films on textiles for all-textile supercapacitors. Toward

this end, Chapter 5 details the steps taken to achieve a POIL film on a textile using iCVD, which had not been achieved previously. Although we initially intended to fabricate POILs on textiles in order to determine their conductivities as a function of temperature and using different counteranions with a polymeric cation, experiments were confined to the first step of determining (a) Which polymers could be successfully iCVD-ed for later simple SN2 solution chemistry to form the POIL and (b) How the POIL(s) could be managed in solution in a way that did not delaminate it(them) from the textile substrate. Investigating both (a) and (b) ultimately hindered any further experimentation due to time constraints. Nonetheless, any progress made is detailed in Chapter 5.

5.2   Poly(ionic) Liquid Thin Films on Fabrics and Threads

Poly(ionic) liquids, or POILs, have found a wide range of applications from solvents and dispersants to actuators, liquid crystals, solar cells, and most importantly for this work, electrolytes. [96,98] Considered a low-temperature organic molten salt, the POILs discussed here are made of a polymeric cation and salt counteranion. One of the most common examples is an imidazolium-type polymer cation backbone stabilized by a salt anion such as a halide, hexafluorophosphate (PF_6^-), tetrafluoroborate (BF_4^-), or bis(trifluoromethanesulfonyl)imide (TFSI⁻). While POILs are ionically conductive by nature, their conductivity can be easily tuned by exchange of the counterion. For example, larger, more organic anions like o-benzoic sulphimide and TFSI⁻ are known to result in higher ionic conductivities because unlike BF_4^- or halide anions, they plasticize the bulk polymer. [99–101] Polymer flexibility is important for increasing ionic conductivity, and it is particularly important in this work for maintaining thin film flexibility on the textile substrate.

One common way to prepare a POIL is free radical polymerization of a non-charged monomer, such as a vinyl imidazole moiety, followed by nucleophilic substitution with an alkyl halide to obtain an imidazolium cation stabilized by the halide anion. [98,102,103] The anion can then be exchanged, usually by heating in solution. This mechanism is illustrated in **Figure 5.1**.

While solution methods in general can be spin- or dip-coated onto solid substrates,
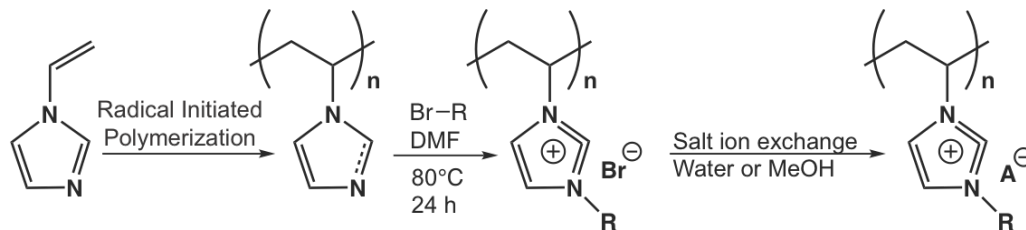
Figure 5.1: Solution method for synthesis of a POIL. Adapted from reference [102].

these methods are unsuitable for the rough surfaces of textiles (see Chapter 4). Therefore, a method using iCVD followed by two simple solution steps was invoked to yield conformal, even films on fabric and thread substrates. However, multiple iCVD reactions were attempted along the way, and ultimately the process for fabrication of POILs on textiles was modified towards a process that (a) Worked in the sense of successfully synthesizing the POIL in solution and/or (b) Did not delaminate the films from the textile completely.

The first step to fabricating a POIL on a textile was iCVD, with the intent to polymerize 1-vinylimidazole directly on the surface of the textile, as has been done for solar cells in the past. [104] However, the reported iCVD conditions did not yield polymer films, nor did adjustments made to the deposition conditions, including lowering stage temperature, increasing deposition pressure, and increasing monomer heating temperature. A less direct method was then sought to iCVD 4-chlorostyrene and post-SN2 exchange the chlorine for imidazole, according to a previously reported method. [102] In this case, the chlorostyrene films were too thin (<175 nm for 30 minute deposition) for practical use due to chlorostyrene itself being difficult to homopolymerize. Although electron-rich and -poor interactions for copolymerization have reportedly increased the deposition rates of 4-chlorostyrene, [105] the only copolymer with which this effect was observed for this project was maleic anhydride. However, the poly(4-chlorostyrene-co-maleic-anhydride) films were too crystalline and inflexible for use as textile POIL material. Conditions for all relevant [failed] iCVD attempts using 1-vinylimidazole and separately 4-chlorostyrene with different copolymers are summarized in **Table 5.1**.

Table 5.1 details the iCVD conditions employed for co-polymerization of 4-chlorostyrene (electron donor) with methyl methacrylate, acrylonitrile, and PFDA, (electron acceptors). Although there is literature precedent for the copolymerizations of some

Table 5.1: Conditions employed for unsuccessful iCVD attempts.

Monomer	Co-monomer	P_{base} (Torr)	P_{dep} (Torr)	$P_{setpoint}$ (Torr)	T_{mon} (°C) T_{co}(°C)	Needle valve turns (mon.; co; init.)	Dep. Time (mins)	Suspected reason for failure
4-chlorostyrene	Methyl methacrylate	.240	.189	---	80 / 65	1;1/2;1/4	20 (03-09-18)	MMA not good e-acceptor
	acrylonitrile	<.300	.3 -.5	---	80 / 25-65	2;1/2;1/4 2;3/8;1/4	10 (3-19-18) 17 (3-19-18)	P_{dep} too low for acrylonitrile
	acrylonitrile	290	varied	1	80 / RT/no heat	1;1/4;1/4	10 min pulse (03-19-18)	P_{dep} too low for acrylonitrile
	PFDA	270	.490	1 (after 1st min)	80 / 80	1/2; 1/2 ;1/4	10 (03-20-18)	PFDA not good e-acceptor
2,4,6,8-tetramethyl-2,4,6,8-tetravinylcyclotetrasiloxane	---	<.300	<.400	---	70	1/8;1/4	20 (12-8 thru 12-20-17) / 10 (03-20-18)	T_{stage} too high / P_{dep} too low
1-vinyl imidazole	---	.292	<.500	---	80	1/4;1/4	30	T_{stage} too high

form of chlorostyrene (2-chlorostyrene or 4-chlorostyrene) with methyl methacrylate and acrylonitrile, [106] and styrene-co-PFDA in supercritical CO_2, [107] none of the similar copolymerizations worked using iCVD. This could be due in part to lack of necessary chamber pressure and stage temperature, both of which in general affect the saturation pressure of the monomer(s) and therein the temperature at which they will adsorb to the substrate surface for polymerization. (See Section 4.2 for saturation pressure details.) In particular, methyl methacrylate and acrylonitrile have high vapor pressures and would therefore require a higher chamber pressure to prevent them being immediately evacuated from the chamber before adsorption to the substrate surface could occur. This type of problem was reported for methyl methacrylate iCVD using a total deposition pressure of 9 Torr, [108] which is much higher than the hundreds of mTorr pressure typically observed for iCVD reactions in this work. Because the vapor pressure of acrylonitrile is much higher than that of methyl methacrylate (109 vs 38.5 mmHg at 25°C, respectively), it is assumed that it too was evacuated before adsorption to the substrate surface could occur, even when the total deposition pressure was fixed at 1 Torr. On the other hand, the PFDA copolymerization with 4-chlorostyrene likely suffered from too high of a deposition pressure (1 Torr). Because

PFDA is so massive and non-volatile, lower deposition pressures are needed to pull it into and through the chamber. Furthermore, the chlorostyrene likely also suffered from too high deposition pressures in this case, as literature reports that 4-aminostyrene was successfully deposited onto various substrates at 0.35 Torr deposition pressure. [109] A similar argument could also be made for the failed 1-vinylimidazole iCVD attempt, wherein the total deposition pressure of 0.50 Torr was slightly too high compared to literature values of maximum 0.35 Torr. [104]

It should be noted here that a thin film of approximately 170 nm thickness of 4-chlorostyrene was deposited on cotton thread (reported in **Table 4.1**) and to it was added a few drops of 1-butylimidazole. The mixture was heated in hexanes at $60^{\circ}C$ overnight in attempt to form a POIL on the thread surface. Although this method may have been successful, the solution dissolved the majority of the thread. After observing the thread dissolution, literature was consulted and revealed that ionic liquids have been used in the past specifically to dissolve cellulose, [110] which suggests futility in developing a POIL on cotton-based substrates. For this reason, all future POIL attempts were made using synthetic fabrics and threads, including nylon and polyester.

Due to the lack of success with iCVD of 4-chlorostyrene and copolymers, 2-chloroethylacrylate was selected as the starting monomer and underwent a reaction similar to that in **Figure 4.2** (here, R=Cl). This polymer (abbreviated "Cl-acryl") was successfully polymerized on multiple occasions, yielding films of approximately 2 microns in thickness over a 10-15 minute deposition period (see **Table 4.1**). However, film solubility and swellability became an issue with time, which may be due to cross-linking within the film due to exposure to light. [111] For example, it was discovered that dissolution in many solvents (N, N-dimethylformamide (DMF), chloroform, acetone, tetrahydrofuran, and even isopropanol) was possible immediately following deposition of the film. However, when the films were stored in closed containers and removed at a later date, solubility was impossible in any of the given solvents. Still, freshly iCVD-ed Cl-acryl films were tested at least once more for solubility, and were also found to be insoluble in the listed solvents, which were reported in literature for these reactions. For this reason, gel permeation chromatography could not be carried out to determine the molecular weights of the polymer films. This lack of solubility

also calls into question the formation of any true POIL species because POILs should be soluble in the more polar solvents, such as isopropanol, DMF, and chloroform.

5.3   Analysis of Attempted POIL Synthesis Reactions

Before the solubility discrepancy was observed, one pathway in particular was followed in attempts to synthesize POILs on textiles. **Figure 5.2** illustrates the assumed reactions. Initially 1-butyl imidazole (Im) was used as the cation-forming species. Free-standing films were tested initially due to solvent/cation-former combinations causing delamination from silicon and polyester substrates. With respect to **Figure 5.2**, a 1-butylimidazole/ethanol solution (1% by volume), the POIL film was (assumed to be) formed post-iCVD via nucleophilic attack on the chloro-acrylate polymer. Ion exchange was then executed to replace the Cl⁻ with TFSI⁻. Ionic conductivities of the resulting thin films were tested via resistance measurements using a Fluke digital multimeter in the absence of a four-point probe. The resistance of a very small (cubic millimiters) POIL film on glass was measured at 12 MΩ. Samples of the films from each reaction step were analyzed using attenuated total reflectance Fourier Transform Infrared Spectroscopy (ATR-FTIR) (model Bruker Alpha). XPS was also used for further characterization of the films, either on glass (Im-TFSI) or on polyester fabric (chloro-acrylate polymer) substrates. All polyester used in this study was polyester lining fabric silk habutae 60 purchased from Fabric Wholesale Direct. **Figure 5.3** shows the XPS (left) and ATR-FTIR (right) spectra.
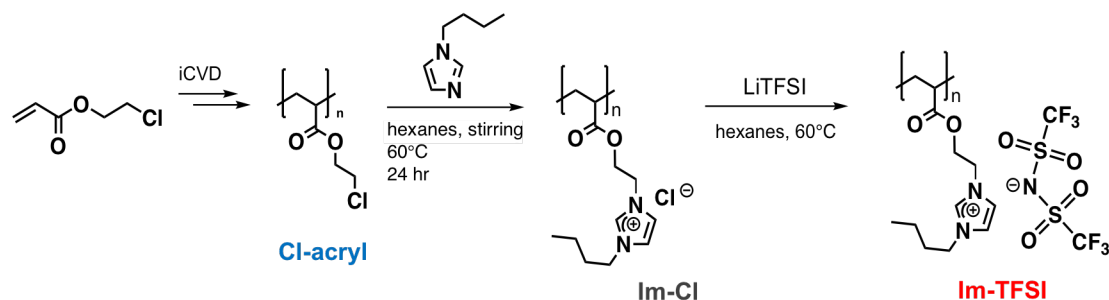
Figure 5.2: Proposed synthesis of a POIL using iCVD, 1-butyl imidazole, and solution exchange of the counteranion.
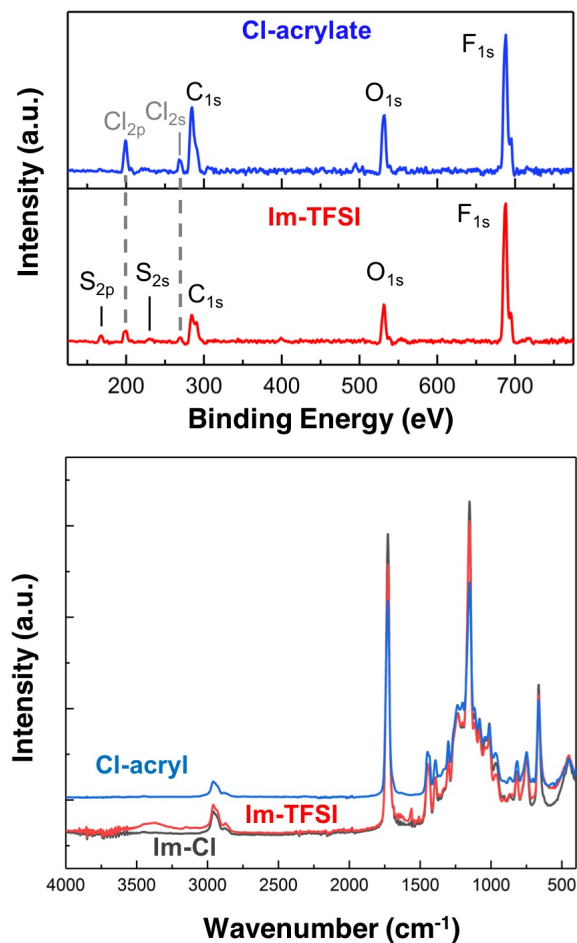
Figure 5.3: XPS of POILs with different anions. **(Top)** XPS of 2-chloroethyl acrylate (blue) and TFSI-exchanged imidazolium POIL assumed from Scheme 5.2 (red). **(Bottom)** ATR-FTIR spectra for assumed species indicated

From the XPS and FTIR data, it can be inferred that the SN2 reaction between the imidazole moiety and the Cl-acryl did not fully take place. The XPS data shows that there is at least some chlorine still present in the TFSI$^-$ -exchanged film, although there are also sulfur peaks that suggest some presence of TFSI$^-$ in the film as well. The FTIR spectrum does not offer significant clarification. The peaks near 3000 cm^{-1} and 3500 cm^{-1} appear to be from the imidazole ring C-H stretch, as reported by other researchers; [104] however, the peaks around 3000 cm^{-1} could also be a result of C-H bonds in the pendant chain that are very close to either chlorine in the Cl-acryl or the imidazole ring in the other two species. The fact that the imidazole films exhibited some small electrical conductivity would suggest that the substitution and subsequent anion exchange reactions were successful

to some degree.

As mentioned, solubility issues with the chloro-acrylate films post-iCVD, assumed to occur due to cross-linking from even a minimal exposure to light, severely limited the swellability and therein the reactivity of the chloro-acrylate films. The film reactivity could be improved by proper preservation via rinsing with a radical scavenger such as butylated hydroxytoluene [112] immediately after iCVD is complete to prevent cross-linking. In the absence of cross-linking, the chloro-acrylate films should at least be swellable and amenable to further reactions in certain polar solvents. The key to keeping the films in place on the textile substrate is to find a solvent that swells the film so that it can react but does not completely dissolve it.

To circumvent issues of chloro-acrylate solubility, a different cation/anion combination could potentially be demonstrated, though still using iCVD as the polymerization step for a conformal polymer coating on textiles. **Figure 5.4**, adapted from reference [112], proposes an alternate method. The cation-former in this method, poly(2-(dimethylamino)ethyl acrylate), has been successfully iCVD-deposited, as indicated in **Table 4.1** in Chapter 4 of this work. Because this method uses an amine-functionalized acrylate in lieu of the chloro-functionalized one, there should be no complications of the film cross-linking under minimal UV exposure, as the chloro-acrylate is assumed to do. Furthermore, the amine functionality could result in easier swellability of the films to undergo the reaction in the second step without completely dissolving in the solvent.
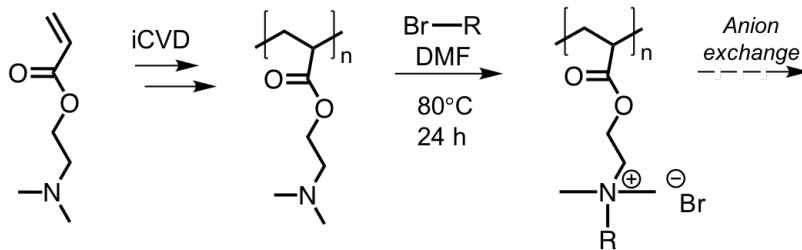
Figure 5.4: POIL synthesis method using 2-(dimethylamino)ethyl acrylate as the starting monomer. Scheme adapted from reference [112].

5.4 Summary

Poly(ionic) liquids could provide a means to enable solid-state supercapacitors on textiles. With this goal in mind, Chapter 5 described two different synthetic pathways for POIL fabrication. Though evidence suggests that the imidazole-based POIL was achieved, the films tended to delaminate from both silicon and textile substrates, rendering them inadequate for textile-based electrolytes. On the other hand, although anion exchange was not successfully demonstrated with the pyrrolidine-based POIL, the films remained adhered to the polyester substrates. Hence, with some optimization, at least one of these techniques could foreseeably deliver successful POIL electrolytes for textile-based supercapacitors.

CHAPTER 6

FUTURE WORK

The goal of this work was to investigate methods for modifying textiles towards smart fabrics, the most useful and robust method being iCVD.The iCVD-related experiments described in this work lay the foundations for other future projects, specifically with triboelectric sensors and all-textile supercapacitor electrolytes, and more generally with new applications such as encapsulation of textile electronic components and fabrication of robust hydrophobic fabrics for water filtration or simply protective clothing purposes.

With regards to the triboelectric sensors described in Chapter 2, iCVD could provide a more advanced method to achieve thinner films encapsulating the conductive threads such that they maintain the feel of the thread rather than the "plastic" feel of the fluoropolymer tape. To further improve the tactile properties of the devices, different polymers with highly negative-tribocharging tendency, such as silicones, could also be investigated. The key here is that iCVD offers both conformality and adhesion to textile substrates along with control over the film thickness. Thus, with the right choice of tribo-active, soft, and flexible polymer(s), one would only need to adjust iCVD conditions to achieve next-generation woven touch sensors. It should also be noted that these films are fundamentally serving as encapsulation to the conductive threads, which is to say they could easily be applied just for that purpose in other textile electronic devices in the future.

With respect to body-motion-sensing textiles such as the elbow sleeve presented in Chapter 3, iCVD could also be useful to improve device performance in terms of strength of the tribo signal and signal to noise ratio. While the knitted, stretchy materials allowed the wearer to move normally, it is possible that they could offer better shielding if functionalized with an ion shield to reduce the effects of ions on the skin surface on charge collection in the electrode materials. It is possible that more densely knitted layers could also add to the shielding effect, although not in such a way as specifically targeted to ions. Nonetheless, further research on the triboelectric sensing component could lead to a more finely tuned sensing garment that is capable of detecting blood pressure, heart beat, or other significant

health metrics.

On a different note, POILs are a relatively new scientific feat with much room for future discovery. Not only can they be intricate and complex in terms of chemical structure, but their behavior in solution and in the solid state is quite unique. For example, Chapter 5 of this work detailed the difficulty in (a) polymerizing and copolymerizing certain species and (b) having to compromise the solid state form for chemical reactivity. For this reason, POILs may require unconventional and/or new processing techniques in order to implement them in textile supercapacitors. However, it may simply be a question of selecting the right copolymers to achieve a solid-state POIL using iCVD alone.

In terms of new processing methods, iCVD may still be the ideal choice, although different types of iCVD polymerization could be explored. For example, studies have been done to develop cationic iCVD for styrene moieties in order to improve deposition rates and minimize waste. A similar cationic initiator would likely be effective in polymerizing the 4-chlorostyrene attempted in Chapter 5, although to achieve a POIL, further chemistry is needed and likely in the solution phase. Nonetheless, iCVD is promising, as Chapter 4 showed it very likely results in more robust functional surfaces than surface grafting with silanes. Therefore, more research could certainly lead to new or simply improved textile surfaces for smart fabrics.

REFERENCES

[1] D.-H. Kim, N. Lu, R. Ma, Y.-S. Kim, R.-H. Kim, S. Wang, J. Wu, S. M. Won, H. Tao, A. Islam, K. J. Yu, T. il Kim, R. Chowdhury, M. Ying, L. Xu, M. Li, H.-J. Chung, H. Keum, M. McCormick, P. Liu, Y.-W. Zhang, F. G. Omenetto, Y. Huang, T. Coleman, and J. A. Rogers, "Epidermal electronics," *Science*, vol. 333, p. 838, 08/12 2011.

[2] J. Sungmook, L. Jongsu, H. Taeghwan, L. Minbaek, and K. Dae-Hyeong, "Fabric-based integrated energy devices for wearable activity monitors," *Advanced Materials*, vol. 26, pp. 6329–6334, 09/18; 2018/04 2014. doi: 10.1002/adma.201402439; 16.

[3] J. Zhong, Y. Zhang, Q. Zhong, Q. Hu, B. Hu, Z. L. Wang, and J. Zhou, "Fiber-based generator for wearable electronics and mobile medication," *ACS Nano*, vol. 8, pp. 6273–6280, 06/24 2014. doi: 10.1021/nn501732z.

[4] A. Pantelopoulos and N. G. Bourbakis, "A survey on wearable sensor-based systems for health monitoring and prognosis," *IEEE Transactions on Systems, Man, and Cybernetics, Part C (Applications and Reviews)*, vol. 40, no. 1, pp. 1–12, 2010. ID: 1.

[5] R. Paradiso, G. Loriga, and N. Taccini, "A wearable health care system based on knitted integrated sensors," *IEEE Transactions on Information Technology in Biomedicine*, vol. 9, no. 3, pp. 337–344, 2005.

[6] L. Yi, Y. B. An, Y. C. Yung, S. Q. Wen, and K. Yi-lin, "Functional design ofsmart-thermalclothing for infants using phase change materialstextiles," 2008.

[7] M. Soleimani, "Knitted switches for smart clothing using double electrode technology," *Sensor Review*, vol. 28, no. 3, pp. 229–232, 2008.

[8] R. Torah, J. L. Ashton, Y. Li, S. Arumugam, H. Sodano, and S. Beeby, "Energy-harvesting materials for smart fabrics and textiles," *MRS Bulletin*, vol. 43, no. 03, pp. 214–219, 2018.

[9] S. Gorgutsa, K. Bachus, S. LaRochelle, R. Oleschuk, and Y. Messaddeq, "Washable hydrophobic smart textiles and multi-material fibers for wireless communication," *Smart Materials and Structures*, vol. 25, no. 11, p. 115027, 2016.

[10] P. Lam, D. Bryson, and J. McCann, "The application of communication technologies in smart clothing," *SMART CLOTHES AND WEARABLE TECHNOLOGY*, no. 83, pp. 205–213, 2009.

[11] C. Winterhalter, J. Teverovsky, P. Wilson, J. Slade, W. Horowitz, E. Tierney, and V. Sharma, "Development of electronic textiles to support networks, communications, and medical applications in future u.s. military protective clothing systems," *IEEE Transactions on Information Technology in Biomedicine*, vol. 9, no. 3, pp. 402–406, 2005.

[12] J. Volakis and A. Kiourti, "Wearable antennas usingelectronictextilesfor rfcommunicationsand medical monitoring," 2016.

[13] J.-H. Lee, H.-S. Cho, S.-H. Park, S. ah Khang, and J.-H. Yang, "An experimental study on the luminescence effects of pof-based flexibletextileusing different methods of weaving andelectronicpackaging focused on the redlight," 2012.

[14] E. Guerel, B. Selm, E. Gürel, M. Rothmaier, R. Rossi, and L. Scherer, "Polymeric optical fiber fabrics for illumination and sensorial applications in textiles," *Journal of Intelligent Material Systems and Structures*, vol. 21, no. 11, pp. 1061–1071, 2010.

[15] A. Taieb, S. Msahli, and F. Sakli, "Design of illuminating textile curtain using solar energy," *The design journal*, vol. 12, no. 2, pp. 195–216, 2009.

[16] H. Ronan, S. Wanchul, and K. Sang-Woo, "Recent progress on flexible triboelectric nanogenerators for selfpowered electronics," *ChemSusChem*, vol. 8, pp. 2327–2344, 07/20; 2018/04 2015. doi: 10.1002/cssc.201403481; 16.

[17] L. McCarty and G. Whitesides, "Electrostatic charging due to separation of ions at interfaces: Contact electrification of ionic electrets," *Angewandte Chemie International Edition*, vol. 47, no. 12, pp. 2188–2207, 2008.

[18] B. Baytekin, H. T. Baytekin, and B. Grzybowski, "What really drives chemical reactions on contact charged surfaces?," *Journal of the American Chemical Society*, vol. 134, no. 17, pp. 7223–7226, 2012.

[19] S. Niu, S. Wang, L. Lin, Y. Liu, Y. S. Zhou, Y. Hu, and Z. L. Wang, "Theoretical study of contact-mode triboelectric nanogenerators as an effective power source," *Energy and Environmental Science*, vol. 6, no. 12, pp. 3576–3583, 2013.

[20] A. F. Diaz and R. M. F. Navarro, "A semi-quantitative triboelectric series for polymeric materials: the influence of chemical structure and properties," *Journal of Electrostatics*, vol. 62, pp. 277–290, November 2004 2004. ID: 271624.

[21] G. Walker, "A review of technologies for sensing contact location on the surface of a display," *Journal of the Society for Information Display*, vol. 20, pp. 413–440, 08/01; 2018/06 2012. doi: 10.1002/jsid.100; 07.

[22] J. Ferri, J. V. Lidón-Roger, J. Moreno, G. Martinez, and E. Garcia-Breijo, "A wearable textile 2d touchpad sensor based on screen-printing technology," 2017. TY: EJOU.

[23] S. Takamatsu, T. Yamashita, T. Imai, and T. Itoh, "Fabric touch sensors using projected self-capacitive touch technique," *Sens. Mater.*, vol. 25, p. 627, 2013.

[24] G. H. Buscher, R. Koiva, C. Schurmann, R. Haschke, and H. J. Ritter, "Flexible and stretchable fabric-based tactile sensor," January 2015 2015. ID: 271599.

[25] M. S. Suen, Y. C. Lin, and R. Chen, "A flexible multifunctional tactile sensor using interlocked zno nanorod arrays for artificial electronic skin," 2016 2016. ID: 278653.

[26] L. K. Baxter, *Capacitive Sensors: Design and Applications*. Hoboken, NJ, USA: Wiley, 1996.

[27] X. Pu, M. Liu, X. Chen, J. Sun, C. Du, Y. Zhang, J. Zhai, W. Hu, and Z. L. Wang, "Ultrastretchable, transparent triboelectric nanogenerator as electronic skin for biomechanical energy harvesting and tactile sensing," *Sci Adv*, vol. 3, 05/01 2017.

[28] Z. Yuan, T. Zhou, Y. Yin, R. Cao, C. Li, and Z. L. Wang, "Transparent and flexible triboelectric sensing array for touch security applications," *ACS Nano*, vol. 11, pp. 8364–8369, 08/22 2017. doi: 10.1021/acsnano.7b03680.

[29] R. Wijesiriwardana, K. Mitcham, W. Hurley, and T. Dias, "Capacitive fiber-meshed transducers for touch and proximity-sensing applications," *IEEE Sensors Journal*, vol. 5, no. 5, pp. 989–994, 2005.

[30] R. Vallett, R. Young, C. Knittel, Y. Kim, and G. Dion, "Development of a carbon fiber knitted capacitive touch sensor," *MRS Advances*, vol. 1, no. 38, pp. 2641–2651, 2016.

[31] J. S. Roh, *Textile touch sensors for wearable and ubiquitous interfaces*, vol. 84. 04/01 2013.

[32] X. Wang, Z. Wang, and Y. Yang, "Hybridized nanogenerator for simultaneously scavenging mechanical and thermal energies by electromagnetic-triboelectric-thermoelectric effects," *Nano Energy*, vol. 26, pp. 164–171, 2016.

[33] K. Lee, H. J. Yoon, T. Jiang, X. Wen, W. Seung, S. W. Kim, and Z. Wang, "Fully packaged self-powered triboelectric pressure sensor using hemispheres-array," *Advanced energy materials*, vol. 6, no. 11, p. 1502566, 2016.

[34] X. Wang, H. Zhang, L. Dong, X. Han, W. Du, J. Zhai, C. Pan, and Z. L. Wang, "Self-powered high-resolution and pressure-sensitive triboelectric sensor matrix for real-time tactile mapping," *Advanced Materials*, vol. 28, no. 15, pp. 2896–2903, 2016.

[35] L. Zhang, Y. Yanhao, G. P. Eyer, S. Guoquan, L. A. Kozik, M. Fairbanks, X. Wang, and T. L. Andrew, "All textile triboelectric generator compatible with traditional textile process," *Advanced Materials Technologies*, vol. 1, p. 1600147, 10/24; 2018/04 2016. doi: 10.1002/admt.201600147; 18.

[36] Y. Xie, S. Wang, L. Lin, Q. Jing, Z. H. Lin, S. Niu, Z. Wu, and Z. L. Wang, "Rotary triboelectric nanogenerator based on a hybridized mechanism for harvesting wind energy," *ACS Nano*, vol. 7, pp. 7119–7125, 08/27 2013. doi: 10.1021/nn402477h.

[37] H. Guo, X. He, J. Zhong, Q. Zhong, Q. Leng, C. Hu, J. Chen, L. Tian, Y. Xi, and J. Zhou, "A nanogenerator for harvesting airflow energy and light energy," *Journal of Materials Chemistry A*, vol. 2, no. 7, pp. 2079–2087, 2014.

[38] Z. L. Wang, J. Chen, and L. Lin, "Progress in triboelectric nanogenerators as a new energy technology and self-powered sensors," *Energy and Environmental Science*, vol. 8, no. 8, pp. 2250–2282, 2015.

[39] Y. C. Lai, J. Deng, S. L. Zhang, S. Niu, H. Guo, and Z. L. Wang, "Single-thread-based wearable and highly stretchable triboelectric nanogenerators and their applications in cloth-based self-powered human-interactive and biomedical sensing," *Advanced Functional Materials*, vol. 27, p. 1604462, 11/03; 2018/04 2016. doi: 10.1002/adfm.201604462; 16.

[40] Y. Mao, D. Geng, E. Liang, and X. Wang, "Single-electrode triboelectric nanogenerator for scavenging friction energy from rolling tires," July 2015 2015. ID: 280655.

[41] Y. Yu and X. Wang, "Chemical modification of polymer surfaces for advanced triboelectric nanogenerator development," *Extreme Mechanics Letters*, vol. 9, pp. 514–530, 2016.

[42] S. J. Montain, S. N. Cheuvront, and H. C. Lukaski, "Sweat mineral-element responses during 7h of exercise-heat stress.," *Int J Sport Nutr Exerc Metab*, vol. 17(6), p. 574, 2007.

[43] S. W. T. III, S. J. Vella, M. D. Dickey, G. K. Kaufman, and G. M. Whitesides, "Controlling the kinetics of contact electrification with patterned surfaces," *Journal of the American Chemical Society*, vol. 131, pp. 8746–8747, 07/01 2009. doi: 10.1021/ja902862b.

[44] T. Elschner, D. Reishofer, R. Kargl, T. Griesser, T. Heinze, T. Grieer, and K. Kleinschek, "Reactive cellulose-based thin films a concept for multifunctional polysaccharide surfaces," *RSC Advances*, vol. 6, no. 76, pp. 72378–72385, 2016.

[45] J. Credou, R. Faddoul, and T. Berthelot, "One-step and eco-friendly modification of cellulose membranes by polymer grafting," *RSC Advances*, vol. 4, no. 105, pp. 60959–60969, 2014.

[46] J. P. F. Lagerwall, C. Schutz, M. Salajkova, J. Noh, J. Park, J. H. Park, G. Scalia, C. Schütz, and L. Bergström, "Cellulose nanocrystal-based materials: from liquid crystal self-assembly and glass formation to multifunctional thin films," *NPG Asia materials*, vol. 6, no. 1, p. e80, 2014.

[47] D. Roy, M. Semsarilar, J. Guthrie, and S. Perrier, "Cellulose modification by polymer grafting: a review," *Chemical Society Reviews*, vol. 38, no. 7, pp. 2046–2064, 2009.

[48] D. Klemm, I. J. Wiley, and Sons, *Comprehensive Cellulose Chemistry, Volume 2 : Functionalization of Cellulose.* Weinheim : Wiley-VCH, volume 2 ed., 1998. Book; Electronic reproduction. Somerset, New Jersey : Wiley InterScience, 2004. Available via World Wide Web.

[49] D. K. Aswal, S. Lenfant, D. Guerin, J. V. Yakhmi, and D. Vuillaume, "Self assembled monolayers on silicon for molecular electronics," 24 May 2006 2006. ID: 271374.

[50] M. J. Owen and D. E. Williams, "Surface modification by fluoroalkyl-functional silanes," *Journal of Adhesion Science and Technology*, vol. 5, no. 4, pp. 307–320, 1991.

[51] G. CHANDRA, "Review of the environmental fate and effects of silicone materials intextileapplications," *Textile Chemist and Colorist*, vol. 27, no. 4, pp. 21–24, 1995.

[52] M. VORONKOV, V. SAMARA, R. EN, A. VA, and V. DYAKOV, "Trialkyl(polyfluoroacyloxy)silanes and their application for anti-adhesion finishing of textile materials," *Zhurnal prikladnoi khimii*, vol. 45, no. 2, pp. 469–+, 1972.

[53] M. VORONKOV, V. DYAKOV, O. FLORENSOVA, and V. MAKARSKAYA, "Modification of cellulosefabricsby trimethyl (polyfluoroacyloxy)silanes," *Journal of applied chemistry of the USSR*, vol. 50, no. 9, pp. 2034–2035, 1977.

[54] K. O. Jang and K. Yeh, "Effects of silicone softeners and silane coupling agents on the performance properties of cotton fabrics," *Textile Research Journal (UK)*, vol. 63, no. 10, pp. 557–565, 1993.

[55] M. Gupta and K. K. Gleason, "Initiated chemical vapor deposition of poly(1h,1h,2h,2h-perfluorodecyl acrylate) thin films," *Langmuir*, vol. 22, pp. 10047–10052, 11/01 2006. doi: 10.1021/la061904m.

[56] M. Gupta and K. K. Gleason, "Surface modification of high aspect ratio structures with fluoropolymer coatings using chemical vapor deposition," *Thin Solid Films*, vol. 517, no. 12, pp. 3547–3550, 2009. J2: Thin Solid Films.

[57] N. Cui, J. Liu, L. Gu, S. Bai, X. Chen, and Y. Qin, "Wearable triboelectric generator for powering the portable electronic devices," *ACS Applied Materials and Interfaces*, vol. 7, pp. 18225–18230, 08/26 2015. doi: 10.1021/am5071688.

[58] Y. Ko, G. Nagaraju, and J. Yu, "Multi-stacked pdms-based triboelectric generators with conductive textile for efficient energy harvesting," *RSC Advances*, vol. 5, no. 9, pp. 6437–6442, 2015.

[59] Z. Lin, J. Chen, and J. Yang, "Recent progress in triboelectric nanogenerators as a renewable and sustainable power source," 2016.

[60] T.-C. Hou, Y. Yang, H. Zhang, J. Chen, L.-J. Chen, and Z. L. Wang, "Triboelectric nanogenerator built inside shoe insole for harvesting walking energy," September 2013 2013. ID: 280655.

[61] Y. Han, Y. Cao, J. Zhao, Y. Yin, L. Ye, X. Wang, and Z. You, "A self-powered insole for human-motion recognition," *Sensors*, vol. 16, p. 1502, 2016.

[62] C. He, W. Zhu, B. Chen, L. Xu, T. Jiang, C. B. Han, G. Q. Gu, D. Li, and Z. L. Wang, "Smart floor with integrated triboelectric nanogenerator as energy harvester and motion sensor," *ACS Applied Materials and Interfaces*, vol. 9, pp. 26126–26133, 08/09 2017. doi: 10.1021/acsami.7b08526.

[63] J. Ma, Y. Jie, J. Bian, T. Li, X. Cao, and N. Wang, "From triboelectric nanogenerator to self-powered smart floor: A minimalist design," September 2017 2017. ID: 280655.

[64] C. Dalsgaard and R. Sterrett, "White paper on smart textile garments and devices: a market overview of smart textile wearable technologies," *Market Opportunities for Smart Textiles, Ohmatex, Denmark*, 2014.

[65] C. Mattmann, F. Clemens, and G. Troster, "Sensor for measuring strain in textile," *Sensors*, vol. 8, no. 6, pp. 3719–3732, 2008.

[66] D. T. Lykken and P. H. Venables, "Direct measurement of skin conductance: A proposal for standardization," *Psychophysiology*, vol. 8, no. 5, pp. 656–672, 1971.

[67] D. V. Knudson, *Fundamentals of Biomechanics*. Kluwer Academic, 2003. 2002040785.

[68] Z. Jan, F. A. Reifler, F. Giuseppino, G. Lutz-Christian, and S. Stefan, "A simple, one-step approach to durable and robust superhydrophobic textiles," *Advanced Functional Materials*, vol. 18, pp. 3662–3669, 11/04; 2018/04 2008. doi: 10.1002/adfm.200800755; 16.

[69] C. Jessen, *Temperature regulation in humans and other mammals.* Springer Science and Business Media, 2012.

[70] A. Wallace, "Burns: some experiences in local care," *British journal of plastic surgery*, vol. 4, pp. 224–229, 1951.

[71] R. W. Picard, "Measuring affect in the wild," in *International Conference on Affective Computing and Intelligent Interaction*, pp. 3–3, Springer, 2011.

[72] S. Khan and A. Malik, *Environmental and Health Effects of Textile Industry Wastewater.* 10/01 2013.

[73] A. Servi, E. G. Burrieza, D. Warsinger, W. Livernois, K. Notarangelo, J. Kharraz, J. H. L. V, H. Arafat, and K. Gleason, "The effects of icvd film thickness and conformality on the permeability and wetting of md membranes," *Journal of Membrane Science*, vol. 523, pp. 470–479, 2017.

[74] A. Coclite, R. Howden, D. Borrelli, C. Petruczok, R. Yang, J. Yagüe, A. Ugur, N. Chen, S. Lee, W. Jo, A. Liu, X. Wang, and K. Gleason, "25th anniversary article: Cvd polymers: A new paradigm for surface modifi cation and device fabrication," *Advanced Materials*, vol. 25, no. 38, pp. 5392–5423, 2013.

[75] G. O. Ince, A. Coclite, and K. Gleason, "Cvd of polymeric thin films: applications in sensors, biotechnology, microelectronics/organic electronics, microfluidics, mems, composites and membranes," *Reports on progress in physics*, vol. 75, no. 1, pp. 016501–016501, 2012.

[76] P. D. Haller and G. Malancha, "Synthesis of polymer nanoparticles via vapor phase deposition onto liquid substrates," *Macromolecular Rapid Communications*, vol. 35, pp. 2000–2004, 12/01; 2018/06 2014. doi: 10.1002/marc.201400436; 14.

[77] C. Cheng and M. Gupta, "Surface functionalization of 3d-printed plastics via initiated chemical vapor deposition," *Beilstein Journal of Nanotechnology*, vol. 8, pp. 1629–1636, 07/05 2017. J1: Beilstein J Nanotechnol.

[78] T. Andrew, L. Zhang, N. Cheng, M. Baima, J. Kim, L. Allison, and S. Hoxie, "Melding vapor-phase organic chemistry and textile manufacturing to produce wearable electronics," *Accounts of Chemical Research*, vol. 51, no. 4, pp. 850–859, 2018.

[79] L. Zhang, M. Fairbanks, and T. Andrew, "Rugged textile electrodes for wearable devices obtained by vapor coating off-the-shelf, plain-woven fabrics," *Advanced Functional Materials*, vol. 27, no. 24, p. 1700415, 2017.

[80] N. Chen, D. H. Kim, P. Kovacik, H. Sojoudi, M. Wang, and K. K. Gleason, "Polymer thin films and surface modification by chemical vapor deposition: Recent progress," *Annual Review of Chemical and Biomolecular Engineering*, vol. 7, pp. 373–393, 06/07; 2018/06 2016. doi: 10.1146/annurev-chembioeng-080615-033524; 24.

[81] P. Moni, A. A. Obeidi, and K. Gleason, "Vapor deposition routes to conformal polymer thin films," *Beilstein journal of nanotechnology*, vol. 8, pp. 723–735, 2017.

[82] M. Ma, Y. Mao, M. Gupta, K. Gleason, and G. Rutledge, "Superhydrophobic fabrics produced by electrospinning and chemical vapor deposition," *Macromolecules*, vol. 38, no. 23, pp. 9742–9748, 2005.

[83] T. Martin, K. K. S. Lau, K. Chan, Y. Mao, M. Gupta, W. S. O'Shaughnessy, and K. Gleason, "Initiated chemical vapor deposition (icvd) of polymeric nanocoatings," *Surface and Coatings Technology*, vol. 201, no. 22-23, pp. 9400–9405, 2007.

[84] N. Cheng, L. Zhang, J. J. Kim, and T. L. Andrew, "Vapor phase organic chemistry to deposit conjugated polymer films on arbitrary substrates," *Journal of Materials Chemistry C*, vol. 5, no. 23, pp. 5787–5796, 2017.

[85] K. Lau, K. K. S. Lau, and K. Gleason, "Initiated chemical vapor deposition (icvd) of poly(alkyl acrylates): An experimental study," *Macromolecules*, vol. 39, no. 10, pp. 3688–3694, 2006.

[86] K. Lau, K. K. S. Lau, and K. Gleason, "Initiated chemical vapor deposition (icvd) of poly(alkyl acrylates): A kinetic model," *Macromolecules*, vol. 39, no. 10, pp. 3695–3703, 2006.

[87] K. Chan and K. K. Gleason, "A mechanistic study of initiated chemical vapor deposition of polymers:,Äâ analyses of deposition rate and molecular weight," *Macromolecules*, vol. 39, pp. 3890–3894, 05/01 2006. doi: 10.1021/ma051776t.

[88] R. Sreenivasan and K. Gleason, "Overview of strategies for the cvd of organic films and functional polymer layers," *Chemical Vapor Deposition*, vol. 15, no. 4-6, pp. 77–90, 2009.

[89] S. H. Baxamusa and K. K. Gleason, "Initiated chemical vapor deposition of polymer films on nonplanar substrates," 30 April 2009 2009. ID: 271603.

[90] N. Garcia, S. Beuermann, M. Buback, T. Davis, N. García, R. Gilbert, R. Hutchinson, A. Kajiwara, M. Kamachi, I. Lacík, and G. Russell, "Critically evaluated rate coefficients for free-radical polymerization, 4," *Macromolecular Chemistry and Physics*, vol. 204, no. 10, pp. 1338–1350, 2003.

[91] K. K. Gleason, ed., *CVD Polymers*. 2015.

[92] J. Bae, J. Park, O. Kwon, and C.-S. Lee, "Energy efficient capacitors based on graphene/conducting polymer hybrids," *Journal of Industrial and Engineering Chemistry*, vol. 51, pp. 1–11, 2017.

[93] X. Lu, M. Yu, G. Wang, Y. Tong, and Y. Li, "Flexible solid-state supercapacitors: design, fabrication and applications," *Energy and environmental science*, vol. 7, no. 7, pp. 2160–2181, 2014.

[94] R. Xu, F. Guo, X. Cui, L. Zhang, K. Wang, and J. Wei, "High performance carbon nanotube based fiber-shaped supercapacitors using redox additives of polypyrrole and hydroquinone," *Journal of Materials Chemistry A*, vol. 3, no. 44, pp. 22353–22360, 2015.

[95] L. Yuan, X.-H. Lu, X. Xiao, T. Zhai, J. Dai, F. Zhang, B. Hu, X. Wang, L. Gong, J. Chen, C. Hu, Y. Tong, J. Zhou, and Z. L. Wang, "Flexible solid-state supercapacitors based on carbon nanoparticles/mno2 nanorods hybrid structure," *ACS Nano*, vol. 6, pp. 656–661, 01/24 2012. doi: 10.1021/nn2041279.

[96] A. S. Shaplov, R. Marcilla, and D. Mecerreyes, "Recent advances in innovative polymer electrolytes based on poly(ionic liquid)s," 1 September 2015 2015. ID: 271355.

[97] O. Green, S. Grubjesic, S. Lee, and M. Firestone, "The design of polymeric ionic liquids for the preparation of functional materials," *Polymer reviews*, vol. 49, no. 4, pp. 339–360, 2009.

[98] D. Mecerreyes, "Polymeric ionic liquids: Broadening the properties and applications of polyelectrolytes," *Progress in polymer science*, vol. 36, no. 12, pp. 1629–1648, 2011.

[99] H. Chen, J.-H. Choi, D. S. de la Cruz, K. Winey, and Y. Elabd, "Polymerized ionic liquids: The effect of random copolymer composition on ion conduction," *Macromolecules*, vol. 42, no. 13, pp. 4809–4816, 2009.

[100] J. Tang, H. Tang, W. Sun, M. Radosz, and Y. Shen, "Poly(ionic liquid)s as new materials for co2 absorption," *Journal of Polymer Science Part A: Polymer Chemistry*, vol. 43, no. 22, pp. 5477–5489, 2005.

[101] W. Qian, J. Texter, and F. Yan, "Frontiers in poly(ionic liquid)s: syntheses and applications," *Chemical Society Reviews*, vol. 46, no. 4, pp. 1124–1159, 2017.

[102] R. L. Weber, Y. Ye, A. L. Schmitt, S. M. Banik, Y. A. Elabd, and M. K. Mahanthappa, "Effect of nanoscale morphology on the conductivity of polymerized ionic liquid block copolymers," *Macromolecules*, vol. 44, pp. 5727–5735, 07/26 2011. doi: 10.1021/ma201067h.

[103] A. Eftekhari and T. Saito, "Synthesis and properties of polymerized ionic liquids," May 2017 2017. ID: 271558.

[104] A. G. Kuba, Y. Y. Smolin, M. Soroush, and K. K. S. Lau, "Synthesis and integration of poly(1-vinylimidazole) polymer electrolyte in dye sensitized solar cells by initiated chemical vapor deposition," 2 November 2016 2016. ID: 271348.

[105] W. E. Tenhaeff and K. K. Gleason, "Initiated chemical vapor deposition of perfectly alternating poly(styrene-alt-maleic anhydride)," 25 September 2007 2007. ID: 271621.

[106] S.-D. Yeo and E. Kiran, "Copolymerization of acrylonitrile with methyl methacrylate and 2-chlorostyrene in supercritical co2," *Macromolecules*, vol. 37, no. 22, pp. 8239–8248, 2004.

[107] D.-J. Park, N.-J. Lee, C.-S. Ha, and W.-J. Cho, "Synthesis and properties of acrylonitrile-epdm-4-chlorostyrene graft copolymer," *Journal of Applied Polymer Science*, vol. 44, no. 4, pp. 727–735, 1992.

[108] K. Chan and K. K. Gleason, "Initiated cvd of poly(methyl methacrylate) thin films," *Chemical Vapor Deposition*, vol. 11, no. 10, pp. 437–443, 2005.

[109] J. Xu and K. Gleason, "Conformal, amine-functionalized thin films by initiated chemical vapor deposition (icvd) for hydrolytically stable microfluidic devices," *Chemistry of Materials*, vol. 22, no. 5, pp. 1732–1738, 2010.

[110] M. Armand, F. Endres, D. MacFarlane, H. Ohno, and B. Scrosati, "Ionic-liquid materials for the electrochemical challenges of the future," *Nature Materials*, vol. 8, no. 8, pp. 621–629, 2009.

[111] A. Robinson and R. Lawson, *Materials and Processes for Next Generation Lithography.* Elsevier Science, 2016.

[112] N. C. for Biotechnology Information, "Butylated hydroxytoluene."